Single cell preparations of *Mycobacterium tuberculosis* damage the mycobacterial envelope and disrupt macrophage interactions

Ekansh Mittal[a,b,1], Andrew T. Roth[c,1], Anushree Seth[d], Srikanth Singamaneni[d,e], Wandy Beatty[b], Jennifer A. Philips[a,b,2]

[a]Division of Infectious Diseases, Department of Medicine, Washington University School of Medicine, St. Louis, MO, 63130, USA.

[b]Department of Molecular Microbiology, Washington University School of Medicine, St. Louis, MO, 63130, USA.

[c]Division of Pulmonary and Critical Care Medicine, Department of Medicine, Washington University School of Medicine, St. Louis, MO, 63130, USA.

[d]Department of Mechanical Engineering and Materials Science, Institute of Materials Science and Engineering, Washington University in St. Louis, St. Louis, MO, 63130, USA.

[e]Siteman Cancer Center, Washington University in St. Louis, St. Louis, MO, 63110, USA.

[1]Equal contribution.

[2]To whom correspondence can be addressed.

Keywords: *M. tuberculosis*, host-pathogen interactions, phthiocerol dimycocerosate, macrophage

Abstract

For decades, investigators have studied the interaction of *Mycobacterium tuberculosis* (Mtb) with macrophages, which serve as a major cellular niche for the bacilli. Because Mtb are prone to aggregation, investigators rely on varied methods to disaggregate the bacteria for these studies. Here, we examined the impact of routinely used preparation methods on bacterial cell envelop integrity, macrophage inflammatory responses, intracellular Mtb survival, and virulence in mice. We found that both gentle sonication and filtering damaged the mycobacterial cell envelope and markedly impacted the outcome of macrophage infections. Unexpectedly, sonicated bacilli were hyperinflammatory, eliciting dramatically higher expression of TLR2-dependent genes and elevated secretion of IL-1β and TNF-α. Despite evoking enhanced inflammatory responses, sonicated bacilli replicated normally in macrophages. In contrast, Mtb that had been passed through a filter induced little inflammatory response, and they were highly attenuated in macrophages. Previous work suggests that the mycobacterial cell envelope lipid, phthiocerol dimycocerosate (PDIM), dampens macrophage inflammatory responses to Mtb. However, we found that the impact of PDIM depended on the method used to prepare Mtb. In conclusion, widely used methodologies to disaggregate Mtb may introduce experimental artifacts in Mtb-host interaction studies, including alteration of host inflammatory signaling, intracellular bacterial survival, and interpretation of bacterial mutants.

Introduction

A fundamental feature of the pathogenesis of *Mycobacterium tuberculosis* (Mtb), the etiologic agent of tuberculosis (TB), is its ability to survive and grow in host macrophages. For more than five decades, many laboratories have investigated how Mtb interacts with and modulates the function of macrophages. Mtb is characterized by a "waxy" coat, which confers its distinctive acid-fast staining properties. The complex cell envelope is important for pathogenesis and also allows Mtb to withstand adverse conditions (Dulberger et al., 2020). The mycobacterial envelope consists of a plasma membrane, peptidoglycan-arabinogalactan layer, outer membrane, and capsular layer (Dulberger et al., 2020). The outermost layers of the envelope are crucial in host-pathogen interactions given that they are directly able to interact with host cells. The capsule is composed primarily of a loose matrix of neutral polysaccharides (Kalscheuer et al., 2019), while the outer membrane is composed of long-chain mycolic fatty acids that are free, attached to trehalose, or covalently attached to the underlying arabinogalactan-peptidoglycan layer. The outer membrane also contains a complex array of unique lipids, such as phthiocerol dimycocerosate (PDIM), phenolic glycolipids, and sulfolipids. Many of these lipids are bioactive; they can intercalate into host membranes, alter inflammatory signaling, disrupt phagosome maturation, and promote mycobacterial virulence (Cambier et al., 2020; Lerner et al., 2018; Quigley et al., 2017). Some outer membrane lipids, such as PDIM, phenolic glycolipids, and sulfoglycolipids, are thought to act as antagonists of pathogen recognition receptors (PRRs) or to shield underlying pathogen associated molecular patterns (PAMPs) to prevent them from activating PRRs (Blanc et al., 2017; Cambier et al., 2014; Reed et al., 2004). Thus, the integrity of the envelope is crucial for host interactions and bacterial virulence.

Given the importance of Mtb-macrophage interactions, a mainstay of the experimental approach of many laboratories is the use of *in vitro* cultured Mtb to infect myeloid cells. However, the tendency of Mtb to form bacterial clumps has long presented an obstacle to these experiments, which depend on using precise and reproducible amounts of bacteria (Wells, 1946). For this reason, low concentrations of detergents are commonly added to culture media, but this does not fully resolve the problem.

Therefore, additional measures are routinely taken to generate single cell suspensions, including sonicating, syringing, centrifuging, filtering, vortexing with glass beads, or some combination of these procedures. The use of these techniques varies widely across different laboratories, the methodology used is not always reported, and there has been little consideration as to how these techniques impact experimental outcomes.

We are interested in how mycobacterial protein and lipid effectors modulate macrophage responses. Sometimes our results differed from published data, leading us to question whether the method of preparing the bacilli explained the differences. However, there was minimal literature into how dispersing mycobacterial clumps impacts the envelope and host-pathogen interactions. Previous studies demonstrated that use of detergent and agitation can release capsular constituents (Lemassu et al., 1996; Sani et al., 2010). In addition, it was reported that Mtb that had been sonicated for 90 seconds were better able to bind to macrophages, and the bacterial envelope appeared uneven and bulging on transmission electron microscopy (Stokes et al., 2004). Another study showed that passing bacterial cultures through 5μm pore filters improved reproducibility of high-throughput antibacterial drug screening compared to vortexing, but the impact on host-pathogen interactions was not assessed (Cheng et al., 2014). Given the lack of published studies addressing our concern, we compared three routinely used methods of preparing single cell suspensions of Mtb: low-speed spin, gentle sonication followed by low-speed spin, or filtration through a 5μm filter. We found that the method of bacterial preparation had a marked impact on intracellular bacterial viability, the global transcriptional pattern of infected cells, macrophage secretion of key innate immune mediators, and the ultrastructure of the bacterial cell envelope. Finally, when comparing an Mtb mutant that lacks PDIM to WT bacilli, we found that the method of preparation had a substantial impact on the inflammatory response to the mutant bacilli.

Results

Macrophage transcriptional responses to Mtb depend on the method of bacterial preparation

To investigate whether the method of dispersing bacterial cultures impacts host responses, we examined gene expression profiles of bone marrow-derived macrophages (BMDMs) that were uninfected or infected with WT Mtb (H37Rv strain) that had been prepared either by passing through a 5μm filter (5μmF) or by brief sonication (so). The sonicated samples underwent three 10-second cycles in a water bath sonicator as described in **Methods**, followed by a low-speed spin (sp) and are designated so/sp. Bacilli prepared by the two methods were added to BMDMs at a multiplicity of infection (MOI) of 5, washed to remove extracellular bacteria after 4 h, and processed for RNA-seq 72 hours post-infection (hpi). We found that 536 genes were differentially expressed between uninfected cells and both of the infected samples (adjusted P value ≤0.01; fold change ≥|2|). Surprisingly, however, there were even more genes that were differentially expressed uniquely in macrophages infected by only one of the two bacterial preparations. 902 differentially expressed genes (DEGs) were unique when we compared uninfected with so/sp-infected macrophages, while 122 genes were uniquely differentially expressed in response to 5μmF bacteria (**Fig. 1A; Supplementary Figure 1A; Supplementary Table 1**). When we compared the DEGs in BMDM infected with so/sp-Mtb to those infected with the 5μmF-preparations, there were 732 DEGs (**Fig. 1A-B**). These included important host defense molecules, including *Il6*, *Nos2*, and *Il1b*, which were markedly higher in so/sp-infected BMDMs compared to 5μmF-infected BMDMs (**Fig. 1B**).

In order to further analyze the transcriptional differences, we used Gene Set Enrichment Analysis (GSEA) to query our expression data against hallmark gene sets from the Molecular Signatures Database (Liberzon et al., 2015). We found that 10 hallmark gene sets were significantly enriched in so/sp preparations relative to 5μmF-infected BMDMs (P ≤0.01; FDR ≤0.01) (**Fig. 1C-D, Supplemental Fig. 1B**). The sonicated bacilli elicited a significant enrichment of gene sets that included TNFA

signaling via NFKB, inflammatory response, MTORC1 signaling, glycolysis, xenobiotic metabolism, and IL6 JAK STAT3 signaling (**Fig. 1C, Supplemental Fig. 1B**). In contrast, 1 hallmark gene set was significantly enriched in 5μmF- relative to so/sp-infected BMDMs (E2F targets) (**Supplemental Fig. 1C**). Visualization of transcriptional data from the hallmark gene set "inflammatory response" showed a distinct gene expression pattern in response to so/sp versus 5μmF bacteria (**Fig. 1D**). Overall, the macrophages infected with the so/sp bacilli displayed a more robust pro-inflammatory phenotype, whereas the 5μmF-infected macrophages were enriched in pro-replication pathways. In addition to the 72 hpi timepoint used for RNA-seq, we found that infection with so/sp Mtb elicited significantly higher levels of expression of *Il1b*, *Nos2*, *Il6* and *Tnf* at 6 and 24 hpi by qPCR compared with 5μmF preparations, with the greatest difference seen early in infection (**Fig. 1E-F**). Strikingly, while the so/sp bacilli markedly upregulated inflammatory gene expression, there was minimal difference between 5μmF-infected and uninfected macrophage 6 hpi and 24 hpi. In these experiments, we used 5μm filters with hydrophilic polyethersulfone (PES) membranes, which are composed of aryl-SO_2-aryl subunits. We considered the possibility that the chemical backbone and hydrophilic nature of the filter might be altering Mtb, but we had similar findings when we used hydrophobic polytetrafluoroethylene (PTFE) filters (**Supplemental Fig. 2A**). In conclusion, the transcriptional response of BMDMs to Mtb infection was markedly different depending on the method of bacterial preparation.

Sonication increases the inflammatory impact of Mtb

Given the dramatic difference between so/sp and 5μmF bacilli, it was important to assess which one more accurately reflects unperturbed Mtb. However, if we were to use Mtb directly from a liquid culture, it would not be possible to establish that we are using similar numbers of bacilli compared to the other preparations given the propensity to clump. Therefore, we used a low-speed spin preparation. This was the same procedure applied to the so/sp sample, but the sonication step was omitted. Specifically, liquid cultures were centrifuged at 206 x g for 10 minutes, after which the supernatant was removed and centrifuged at 132 x g for 8 minutes, and the final supernatant was used to infect BMDMs. We found

that macrophages infected with the spin (sp) sample had an intermediate phenotype between so/sp and 5μmF samples (**Fig. 2A**), eliciting significantly less *Il1b*, *Il6*, *Nos2*, and *Tnf* expression than the so/sp samples. A variety of Mtb PAMPs have been shown to activate TLR2 (Hinman et al., 2021). In order to establish whether the so/sp samples were activating TLR2-dependent pathways, we infected BMDMs from *Tlr2*$^{-/-}$ mice. We found that expression of *Il1b*, *Il6*, *Nos2*, and *Tnf* were significantly reduced in TLR2 KO BMDMs in response to so/sp Mtb relative to WT BMDMs (**Fig. 2B**). This was also true for the induction observed in response to spin preparations.

We wondered if the 5μmF bacilli contained a factor that inhibited macrophage gene expression or if they were just less proinflammatory. To address this, we mixed so/sp and 5μmF bacilli together in equal proportions and assayed gene expression by qPCR. We found that the mixed samples were still inflammatory, arguing against a potent inhibitory factor coming from the filtered preparation (**Supplemental Fig. 2B**). In addition, if we prepared bacteria by first sonicating and then using a 5μmF (so/5μmF), the expression changes resembled so/sp infection, with marked upregulation of *Il1b*, *Il6*, *Nos2*, and *Tnf* (**Fig. 2A**). We considered the possibility that the different inflammatory responses might be a result of different degrees of aggregation of the bacilli in each preparation. To visualize the bacteria, we infected BMDMs with GFP-expressing Mtb prepared by the various methods and examined them by fluorescence microscopy. We found that the bacilli from the 5μmF preparation were uniformly composed of single cells, while small clumps were routinely seen in both the so/sp and sp samples (**Fig. 2C**). Thus, one possibility was that clumps are more inflammatory, but when the sonicated sample was filtered (so/5μmF), there were no clumps, and the bacilli still induced high levels of *Il1b*, *Il6*, *Nos2*, and *Tnf* (**Fig. 2A-C**). To investigate whether the response to sonicated bacteria was due to soluble factors released from the bacilli, we passed the so/sp sample through a 0.2 μm filter to remove bacteria. We treated macrophages with equal volumes of the sterile filtrate or the unfiltered so/sp sample, and analyzed subsequent gene expression. In support of extra-bacterial components contributing to the inflammatory gene expression, the expression of *Il1b, Nos2, Il6, and Tnf* were all significantly increased

in response to the sterile filtrate prepared from the so/sp bacteria compared to uninfected BMDMs (**Fig. 2D**). In contrast, there was no difference in expression of these genes in the sterile filtrate of 5μmF bacteria relative to uninfected BMDMs (**Fig. 2D**). To conclude, compared to bacteria prepared by a low-speed spin or 5μmF, bacilli that were sonicated induced substantially higher TLR2-dependent transcriptional responses in macrophages, independent of their aggregation status and due in part to soluble mediators.

To determine whether the changes in gene expression resulted in altered cytokine secretion, we used the FluoroDOT assay to evaluate secretion of TNF-α. This approach uses plasmon-enhanced fluorescent nanoparticles called plasmonic fluors to visualize protein secretion by microscopy (**Supplemental Fig. 3**). This allowed us to examine secretion of TNF-α at an early time point after infection and with single cell resolution (Liang et al., 2021). Similar to the transcriptional data, the sonicated preparations elicited the most TNF-α secretion followed by the sp and 5μmF preparations (**Fig. 3A-B**). We confirmed these findings by measuring TNF-α by enzyme linked immunosorbent assay (ELISA; **Fig. 3C**). We also evaluated IL-1β secretion using ELISA and found that the so/sp preparation elicited increased secretion of IL-1β **(Fig. 3C**). Interestingly, we found that when infected by the sonicated samples, most of the macrophages, both infected as well as uninfected bystanders in the same well, secreted TNF-α. In contrast, infection with the sp or 5μmF Mtb resulted in only infected cells secreting TNF-α (**Fig. 3A-B**). In addition, so/sp samples that had been sterilized by passage through a 0.2 μm filter elicited significantly more TNF-α secretion than sterilized 5μmF samples (**Fig.3D-E**). This is consistent with the observation that extra-bacterial components in the sonicated preparation contribute to inflammatory gene expression.

Filtered Mtb are markedly attenuated in BMDMs but not in AMs or mice

Given that the different preparations generated pronounced differences in macrophage gene expression and cytokine secretion, we hypothesized that they would also exhibit differences in

intracellular viability. We infected BMDMs with Mtb prepared by the different methods, and the intracellular bacilli were enumerated at 4 hpi and 5 days post-infection (dpi). Mtb that were prepared by so/sp or sp were able to grow in macrophages, a defining feature of Mtb pathogenesis (**Fig. 4A**). In contrast, the filtered bacteria (so/5μmF and 5μmF) failed to grow. While the transcriptional profile in response to so/5μmF bacteria resembled so/sp bacteria, their growth was equally attenuated as the 5μmF bacteria, suggesting that filtering was destructive to the bacteria. Increasing the MOI of the filtered bacteria to 20 or 40 did not overcome the intracellular growth defect. We verified that the filtered Mtb were still viable, as they grew indistinguishably from other preparations when they were inoculated in liquid culture (**Supplemental Fig. 2C**). In addition, filtered bacteria were able to grow in alveolar macrophages, which are more permissive to Mtb growth than BMDMs (**Fig. 4B**). Thus, filtered Mtb appeared to have lost the ability to counter the antimicrobial properties of BMDMs.

To assess whether different bacterial preparation alter outcomes *in vivo*, we infected C57BL/6 mice with different bacterial preparations of Mtb using the low-dose aerosol model of infection. We found that we had to use twice as many 5μmF bacilli in the nebulizer to achieve the same number of bacteria in the lung on the day after infection. We did not find any significant difference in whole-lung CFU from lung 7 or 14 days dpi or from spleens at 14 dpi (**Fig. 4C-D**). Further, the whole-lung expression of IL-1β, IL-6, and TNF-α were the same irrespective of bacterial preparation method (**Fig. 4E-F**). In conclusion, although the aerosol inoculum had to be adjusted to achieve the same starting dose of the 5μmF bacteria, we observed no differences in growth of Mtb in the lungs or spleen during the first two weeks of infection and no differences in expression of pro-inflammatory cytokines based upon preparation method.

Sonication and filtering affect the bacterial cell wall

To determine if there were structural differences between the sonicated, spun, and filtered Mtb, we used transition electron microscopy (TEM). We first generated ultrathin cross-sections of bacteria to visualize

the ultrastructure of the cell envelope (**Fig. 5A-C**). In bacteria prepared with low-speed spin, we could distinguish the structural layers of the cell envelope that have been previously described: the innermost phospholipid bilayer, followed by electron-dense peptidoglycan and arabinogalactan layers, a translucent mycobacterial outer membrane, and an outermost carbohydrate-rich capsular layer (**Fig. 5B)**. In bacteria prepared with sonication, all of these distinct layers were apparent (**Fig. 5A**). In the 5μmF-prepared bacteria, the phospholipid bilayer was seen, surrounded by an electron dense layer, but there appeared to be loss of the capsular layer and potentially the mycomembrane as well (**Fig. 5C**). While TEM of ultrathin cross-sections provided excellent resolution of the cell wall, it was also subject to artifact introduced by drying and fracturing of the bacteria required in this technique. This made it difficult to know how representative the well-preserved bacilli were in terms of the total population. Therefore, we also visualized bacilli by adsorption to a copper grid followed by 1% uranyl acetate staining, a simple technique which minimized artifact (**Fig. 5D-F**). Uranyl acetate is a common negative stain used for TEM that can bind to capsular polysaccharides (Stukalov et al., 2008), and it created an electron dense halo around the bacteria. The prominent electron dense halo was seen on the majority of so/sp and low-speed spin bacteria (**Fig. 5D-E**), but absent from most bacteria prepared with the 5μmF (**Fig. 5F**). This suggests a different chemical composition of the outermost layer of the filtered bacteria and was consistent with the differences noted in the TEM. In addition, the samples from 5μmF-treated bacteria had substantial extracellular debris, which may be damaged fragments from the outer layers of the envelope. Finally, more dead bacteria were noted in the 5μmF sample as evidenced by penetration of the dark staining uranyl acetate into the cells. Using this technique, we also observed that the so/sp bacteria, but not sp or 5μmF bacteria, had prominent round protuberances that were approximately 0.2 to 1 μM in diameter present on the outer surface of the bacteria or, less frequently, in the culture filtrate. To conclude, both sonicated and filtered preparations had EM evidence of distinct types of damage to the envelope that were not apparent in the samples which had been prepared by centrifugation.

The interpretation of the role of PDIM in inflammatory responses depends upon preparation method

PDIM is a multifunctional virulence lipid that is present in the envelope of members of the Mtb complex as well as closely related *Mycobacterium marinum*. Along with the ESX-1 type VII secretion system, PDIM facilitates phagosomal escape of Mtb, a crucial event that allows the bacteria to gain access to the cytosol, subvert cell death pathways, and promote extracellular spread (Augenstreich et al., 2017; Barczak et al., 2017; Cox et al., 1999; Lerner et al., 2018; Osman et al., 2020; Quigley et al., 2017). In addition, PDIM contributes to the low permeability of the mycobacterial envelope, alters the host's initial innate immune response, and may physically shield mycobacterial PAMPs or interfere with their activation of PRRs (Astarie-Dequeker et al., 2009; Camacho et al., 2001; Cambier et al., 2014; Murry et al., 2009; Rousseau et al., 2004; Siméone et al., 2007). To determine whether PDIM dampens inflammatory signaling, we used a strain with a deletion in *ppsD*, which results the in the absence of PDIM (Barczak et al., 2017). When we examined macrophage gene expression after infection with Δ*ppsD* by qPCR, we found that expression of *Il1b*, *Il6*, *Nos2*, and *Tnf* was significantly increased compared to infection with WT Mtb, consistent with the idea that PDIM reduces inflammatory signaling (**Fig. 6A**). However, this was only in the sonicated sample; there was no difference between Δ*ppsD* and WT Mtb if they were prepared by sp or 5μmF. We had similar findings when we used the FluoroDOT assay to examine TNF-α secretion (**Fig. 6B**). The Δ*ppsD* mutant elicited more TNF–α secretion than WT Mtb, but only if the sample was sonicated. Interestingly, when we examined the Δ*ppsD* mutant by EM, we found that the Δ*ppsD* mutant lacked the dark halo that was seen in so/sp and sp samples of WT Mtb; the halo was restored by complementation, suggesting that lack of PDIM altered the interaction of uranyl acetate with the mycobacterial surface (**Fig. 6D-I**). This difference, however, is unlikely to account for the hyperinflammatory signaling, as it was seen in all Δ*ppsD* samples, and only the sonicated samples were hyperinflammatory. As we had seen with WT Mtb, there were round protrusions and vesicles in sonicated sample of both Δ*ppsD* and the complemented strain. There was no obvious visual difference between the Δ*ppsD* mutant and complemented strain to explain why the so/sp Δ*ppsD*

mutant was more hyperinflammatory than so/sp WT. To conclude, the hyperinflammatory phenotype associated with the Δ*ppsD* mutant depended upon the method of bacterial preparation.

Discussion

For decades, investigators have studied the interaction of Mtb with macrophages. They have also employed a variety of methods to disperse the bacilli to enable subsequent analysis. We found that two commonly used single cell preparation methods significantly impact Mtb-host interactions; both gentle sonication and filtering resulted in visual evidence of cell envelope damage on electron microscopy. Unexpectedly, sonicated bacilli were hyperinflammatory, and filtered Mtb were highly attenuated in macrophages. In addition, we found that the impact of PDIM on the early macrophage transcriptional responses to Mtb depended on the method of preparation. Loss of PDIM had no impact on pro-inflammatory responses to centrifuged or filtered bacteria, but it resulted in increased pro-inflammatory gene expression if the bacteria were briefly sonicated. This suggests that the PDIM mutant is either more sensitive to the sonication-induced damage or that it is more inflammatory once that damage occurs. It is important to point out that we only examined the early TLR2-dependent response. PDIM influences a variety of processes, including later TLR2-driven responses, phagosomal escape, and intracellular survival (Augenstreich et al., 2017; Barczak et al., 2017; Cambier et al., 2020; Hinman et al., 2021; Lerner et al., 2018; Osman et al., 2020; Quigley et al., 2017). It is possible that these processes are independent of preparation methods. Nonetheless, our studies demonstrate that the preparation method needs to be considered in host-pathogen interaction studies, as it can change the interpretation of bacterial mutants and has a dramatic effect on TLR2-dependent responses and intracellular bacterial survival.

We found that Mtb growth in mice was not impacted by the preparation method. This might be explained by the observation that although filtered bacilli were highly attenuated in BMDMs, they grew normally in AMs, the first myeloid cells that Mtb encounters in the lung (Cohen et al., 2018). It is notable that the filtered bacteria, which appear stripped of the outer layers of the envelope, were able to establish

infection and grow in AMs, highlighting the permissiveness of the first line of defense against Mtb. AMs are poised to suppress inflammatory responses to foreign material in order to prevent lung injury, and they seem poorly equipped to control Mtb infection (Huang et al., 2018; Lavalett et al., 2017; Pisu et al., 2020; Rothchild et al., 2019). By the time the bacilli enter more restrictive macrophage populations, they may have recovered from the *in vitro* procedures and adapted to the *in vivo* environment. We did find that we had to use 2-fold more filtered bacteria in the aerosol machine to achieve the same number of Mtb in the lungs as so/sp and sp preparations. This suggests that filtered bacteria may be less able to survive aerosolization or the environment in the airways, although there are a variety of other possibilities as well.

Given the extensive use of macrophages in Mtb pathogenesis studies, there are surprisingly few studies investigating the impact of dispersal methods. A 2004 study demonstrated that prolonged sonication (5 minutes) reduces Mtb viability, while bacteria that had undergone gentle sonication (30 sec x 3) exhibited enhanced binding to macrophages and altered surface charge relative to syringed bacteria (Stokes et al., 2004). In that study, the sonicated bacteria had an altered cell envelope, which appeared uneven and bulging. Even though we sonicated for a shorter time (10 sec x 3), we also saw evidence of similar cell envelop disruption by TEM. In addition, sonicated bacteria elicited orders-of-magnitude higher levels of TLR2-dependent transcriptional responses, leading to enhanced IL-1β and TNF-α secretion. This was mediated in part by material that was no longer cell associated, as even sterile-filtered samples activated macrophages. In addition, uninfected bystander cells that had been treated with so/sp preparations secreted TNF-α in the FluoroDOT assay. Our TEM findings suggest that sonication results in cell envelope damage and generation of small structures that resemble extracellular vesicles (EVs) that have been described in Mtb, although the vesicles that we saw are generally larger than the majority of EVs (Prados-Rosales et al., 2011). Mtb EVs are formed by an active process and contain immunomodulatory molecules including lipoarabinomannan and other TLR2 agonists (Athman et al., 2015; Palacios et al., 2021; Prados-Rosales et al., 2011). Whether the

structures formed by sonication have similar content to EVs found in growing cultures will require further studies.

While our study was limited to three common single cell preparation methods, we expect that other techniques would also impact the mycobacterial envelope and host interactions. We queried PubMed for papers published in 2021 on Mtb and macrophages to determine what methods were commonly used (**Supplemental Fig. 4**). Of the 119 papers, only 39.5% reported how they generated single cell suspensions. Of those that did report their methodology, 42.5% used more than one method. The most commonly reported methods were syringing, followed by sonication and low-speed centrifugation. Less often, filtering, vortexing with glass beads, or allowing gravity to sediment the larger clumps were used. Dispersing clumps with glass beads would likely disrupt the envelope, as studies have used this technique to selectively remove and isolate the capsular layer to analyze its components (Lemassu & Daffe, 1994; Lemassu et al., 1996; Ortalo-Magne et al., 1995). Others have reported that syringing through a 25-gauge needle produced no apparent disruption to the envelope on TEM (Stokes et al., 2004), but these samples were not evaluated further in terms of macrophage responses. We did not evaluate syringing, because it is not an approved method in our biosafety level 3 facility due to the risk of aerosolization and needle stick injuries. The physical forces used to disrupt clumps by this method might also result in envelope alterations, and investigators should consider this in their studies. Overall, we consider centrifuged samples as the least disrupted, but even centrifugation might disrupt the capsule, as do detergents that are commonly used in liquid cultures (and were used for all of our studies). Detergents are known to cause release of capsular components into the culture filtrate (Kalscheuer et al., 2019; Sani et al., 2010), although the impact on host interactions is relatively unexplored. The impact of detergent treatment on cytokine responses and vaccine responses have been evaluated, but after detergent treatment, single cell suspensions were generated by filtering, sonicating, or syringing (Prados-Rosales et al., 2016; Sani et al., 2010), complicating the interpretation.

Even if investigators had a non-disruptive way to isolate single cells, this relatively minor population may not reflect the behavior of small or large aggregates that make up a large fraction of the bacterial population. The aggregation state of Mtb has long been reported to be important to pathogenesis. For example, the observation that Mtb forms serpentine cords *in vivo* dates back to the earliest descriptions of the bacteria. Aggregated Mtb are found at the periphery of human necrotic granulomas, in alveolar macrophages of Mtb-infected patients, and are exhaled by infected individuals (Dinkele et al., 2021; Rodel et al., 2021; Ufimtseva et al., 2018). Initially, we considered that one explanation for our findings was that there are different degrees of aggregation in the different bacterial preparations (Rodel et al., 2021). We found that so/sp and sp samples contained more clumps than 5μmF-prepared bacilli, but the clumps cannot account for the hyperinflammatory phenotype because when the sample was subsequently filtered (so/5uF), the aggregates were removed, but it was still hyperinflammatory. In addition, the literature describing the impact of aggregation on host interactions is difficult to interpret in light of our findings, as many of these studies used agitation with glass beads, filtration, sonication, or some combination of these procedures to generate the dispersed samples (Kolloli et al., 2021; Mahamed et al., 2017; Rodel et al., 2021). Thus, the aggregation of bacilli is likely an important virulence property of Mtb, which is overlooked in the effort to generate single cell suspensions. However, in generating single cell suspensions, investigators also introduce the potential for experimental artifact. It is possible that experimental differences in how other laboratories sonicate or filter bacteria could mitigate the effects that we found. We used log phase cultures of the H37Rv strain that had been grown with gentle agitation, a fatty acid source (oleic acid), and 0.05% Tyloxapol to infect murine macrophages, but other investigators use different strains, frozen stocks, omit oleic acid, use different detergents, or infect human macrophages, all of which could lead to differences from our findings. Based upon our findings, we encourage investigators to fully report the methods that they use to grow and process mycobacteria and consider the impact of the methodology on their findings.

While sonication is an artificial stimulus, our findings highlight the massive pro-inflammatory potential of Mtb that is kept in check by the organization and integrity of the envelop. We imagine that by altering

cell envelop architecture, Mtb tune their interactions to achieve the desired host response (Garcia-Vilanova et al., 2019); for example, for initial infection and persistence, it may benefit the bacilli to minimize the TLR2-driven inflammatory response to promote immune evasion, whereas in order to drive tissue pathology and transmission, the bacilli may generate a hyperinflammatory phenotype. While the Mtb cell wall is known to be dynamic (Dulberger et al., 2020), little is known about the structure and function of the cell wall during different *in vivo* contexts. To this end, a recent study evaluated the ultrastructure of the Mtb cell wall *ex vivo* from infected human sputum samples (Vijay et al., 2017). The characteristic three layers were found, and a reduction in the electron translucent layer was noted when bacilli were grown under stress conditions. Further *in vivo* studies investigating how Mtb regulates cell envelop architecture to modulate host responses and deploy virulence lipids and protein effectors are needed.

Materials and Methods

Bacterial Strains and Growth Conditions

The Mtb strains H37Rv (WT), Δ*ppsD*, and Δ*ppsD::ppsD* were used in this study. The Δ*ppsD* and Δ*ppsD::ppsD* strains were from A. Barczak and previously described (Barczak et al., 2017). Bacteria were grown to mid-log phase in an incubator at 37°C with 5% CO_2 and gentle agitation (120 rpm). Bacteria were grown in 7H9 media supplemented with Middlebrook OADC (oleic acid, albumin, dextrose, catalase), 0.05% Tyloxapol, and 0.2% glycerol. H37Rv Δ*ppsD* growth media was additionally supplemented with 50 μg/mL hygromycin, GFP-expressing bacterial strains with 25 μg/mL kanamycin, and H37Rv Δ*ppsD*::*ppsD* with 50μg/mL hygromycin and 25μg/mL kanamycin.

Generation of single cell suspensions of Mtb

Following growth of Mtb to mid-log phase (OD_{600} 0.5-0.8), bacteria were washed with phosphate-buffered saline (PBS) and resuspended in the appropriate media for the subsequent study. Single cell suspensions of Mtb were generated using one or a combination of the following methods: 1) low-speed spin (sp): bacteria were centrifuged at 206 x g for 10 min followed by 132 x g for 8 min, with the

supernatant collected following each spin; 2) 5μm filter (5μmF): 6-20 ml of bacterial culture were added to a 10 mL syringe and then, with gentle pressure, passed through a 5μm polyethersulfone (PES) filter (PALL Life Sciences; cat. 4650) except in the case were polytetrafluoroethylene (PTFE) filters (Tisch scientific; cat. SF17400) were used; 3) sonication (so): 4-10 ml bacteria in a 15 ml conical tube were placed in a water bath sonicator (Branson Ultrasonics Corporation, Digital Sonifier 450) and sonicated with three pulses lasting 10 s each, with an amplitude of 80% and 5 s rests between each pulse. Following sonication, bacteria were centrifuged with a low-speed spin (so/sp) or passed through a 5μm filter (so/5μmF), as described above. Following the preparations described above, the concentrations of bacterial suspensions with OD_{600} between 0.04-0.12 were calculated using the formula: 1 OD_{600} = 3 x 10^8 bacteria per mL. For some experiments, bacterial cultures were further passed through a 0.2 μm filter (PALL Life Sciences; cat. 4652).

Mice

8 to 12 week-old C57BL/6J and *Tlr2*$^{-/-}$ (B6.129-Tlr2tm1Kir/J) mice were obtained from The Jackson Laboratory. Mice infected with Mtb were housed in a biosafety level 3 containment suite. All work with mice were approved by the Washington University School of Medicine Institutional Animal Care and Use Committee. Euthanasia was performed in accordance with the 2020 *AVMA Guidelines for the Euthanasia of Animals* prior to tissue harvest.

Bone marrow-derived macrophage isolation and infection

Mouse hematopoietic stem cells were isolated as described in (Banaiee et al., 2006). Hematopoietic cells were differentiated by culturing for 7 days in Dulbecco's Modified Eagle Medium (DMEM) with 10% FBS, 2 mM L-glutamine, and 1 mM pyruvate (DMEM complete). DMEM complete media was supplemented with 20% L929 cell supernatant (as a source of macrophage colony stimulating factor (M-CSF), 100 U/mL final concentration), 10 units/ml penicillin, and 10 units/ml streptomycin. Following differentiation, BMDMs were washed with PBS, resuspended in DMEM complete with 10% L929 cell

supernatant, and plated for infection the following day. Single cell suspensions of Mtb in DMEM complete with 10% L929 added to macrophages at a MOI of 5, 10, 20, or 40, and plates were spun for 5 minutes at 51 x g. The MOI was verified by plating the inoculum. At 4 hpi, macrophages were washed 3 times with DMEM to remove extracellular bacteria. To enumerate CFU, at specified time points macrophages were lysed with 0.06% sodium dodecyl sulfate (SDS) in water and serially diluted in PBS. The cell lysates were plated on 7H11 agar plates supplemented with OADC and glycerol, and CFU were counted after 14-21 days. For qPCR, macrophages were lysed in TRI Reagent (Zymo Research, R2050-1-50), and total RNA was extracted.

Alveolar macrophage isolation and infection

Mice were euthanized with 1 mg isofluorane instilled in a cotton ball. The trachea was exposed, incised with a small horizontal cut, and cannulated with an 18-gauge catheter. 8 washes with 1 mL wash buffer (ice-cold PBS, 2 mM EDTA, 1% FBS) were performed. Cells were washed and seeded in alveolar macrophage media [DMEM with 10% L929 cell supernatant, 10% FBS, 1 mM pyruvate, and 10 mM N-2-hydroxyethylpiperazine-N'-2-ethanesulphonic acid (HEPES)] and infected the same day as described above for BMDM infections.

RNA sequencing

Mouse hematopoietic cells were collected and differentiated to BMDMs as above. 1.6 x 10^6 BMDMs per well were incubated overnight in a six-well plate. BMDMs were either uninfected or infected at a MOI of 5 with Mtb prepared by the designated single cell preparation method. 5 samples per group were used. At 72 hpi, macrophages were lysed in TRI Reagent and total RNA was extracted. Total RNA integrity was determined using Agilent Bioanalyzer or 4200 Tapestation. Library preparation was performed with 500ng to 1ug total RNA. Ribosomal RNA was removed by an RNase-H method using RiboErase kits (Kapa Biosystems). mRNA was then fragmented in reverse transcriptase buffer and heating to 94°C for 8 min. mRNA was reverse transcribed to yield cDNA using SuperScript III RT enzyme (Life Technologies, per manufacturer's instructions) and random hexamers. A second strand reaction was

performed to yield ds-cDNA. cDNA was blunt ended, had an A base added to the 3' ends, and then had Illumina sequencing adapters ligated to the ends. Ligated fragments were then amplified for 12-15 cycles using primers incorporating unique dual index tags. Fragments were sequenced on an Illumina NovaSeq-6000 using paired end reads extending 150 bases. The raw CPM values that were generated underwent filtering, with removal of mitochondrial RNA, autosomal rRNA, and low-expressed genes with less than 1 CPM in the smallest group size, followed by Voom transformation of counts. Differentially expressed genes were then determined using the "limma" package from bioconductor.org. Heatmaps were generated in R using the "pheatmap" package.

Gene set enrichment analysis

We imputed normalized gene expression data and associated Ensembl Stable IDs of differentially expressed genes from our RNA-seq experiment into GSEA software. GSEA then analyzed our dataset for enriched genetic signatures curated in the hallmark gene sets by the Molecular Signatures Database (Liberzon et al., 2015; Subramanian et al., 2005). Genes were ranked based on their expression and compared against the hallmark gene sets in order to generate an enrichment score. A nominal P value was then generated followed by normalization for the size of the gene set and adjustment for multiple hypothesis testing to yield a false discovery rate (FDR) as previously described (Subramanian et al., 2005). Gene sets which had a P-value <0.01 and an FDR <0.01 were considered significant.

Quantitative Polymerase Chain Reaction

BMDMs (2.0×10^5) were plated in 24 well plates. At indicated time points, macrophage growth media was aspirated, and 100μL TRIzol (Zymo Research, R2050-1-50) was added to each well followed by isolation of total RNA using Direct-Zol RNA Mini-Prep Plus Kit (Zymo Research, R1058) according to the manufacturer's instructions. RNA concentrations were determined using NanoDrop One (ThermoScientific), and cDNA was made with High Capacitance cDNA Reverse Transcription Kit (Thermo-Fisher). Quantitative PCR was performed using SYBR Green dye (Bio-Rad CFX Connect

Real-Time System). Fold-changes in gene expression were calculating by normalizing data to *Gapdh* as a house-keeping gene and values were presented relative to uninfected cells. For analysis of whole lung gene expression, the left lungs were placed in 800 μL TRIzol and lysed using bead beating with 3.2 mm stainless steel beads (BioSpec Products) with three 90 s cycles. Samples were cooled on ice between cycles. Samples were centrifuged at 15,000 x g for 5 min; the supernatant was filtered through 0.22 μm filters and used to isolate total RNA with the Direct-Zol RNA Mini-Prep Plus Kit. The nucleotide sequences of all primers used are presented in **Supplemental Table 2**.

Fluorescence microscopy

BMDMs (3 X 10^4) were seeded in glass bottom 96-well plate (Ibidi, catalog number 89626) and infected with GFP-expressing H37Rv at a MOI of 5. After 4 h, macrophages were washed with PBS and fixed with 1% paraformaldehyde in PBS overnight followed by permeabilization in 0.1% vol/vol Triton X-100 (Millipore Sigma) in PBS for 10 min at room temperature (RT) and blocked for 45 min in 2% bovine serum albumin (BSA) in PBS prior to staining with DAPI (4=,6-diamidino-2-phenylindole) and mounted in Prolong Diamond antifade (Molecular Probes, Life Technologies). Images were captured using a Nikon Eclipse Ti confocal microscope (Nikon Instruments, Inc.) equipped with a 60X apochromat oil objective lens. Image acquisition was done using NIS-Elements version 4.40.

ELISA

For *in vitro* samples, 2.0 x 10^5 BMDM in 24 well plates were infected with Mtb at a MOI of 10. At the indicated timepoints, the cell supernatant was collected and filtered through 0.22 μm filters. For lung samples, tissue was homogenized in 2mL PBS, centrifuged at 400 x g for 5 min to pellet cellular debris, then the supernatant was filtered using a 96-well 0.22 μm filter plate. Cytokines were measured from the supernatant with R&D Systems DuoSet ELISA kits for TNF-α, IL1B, and IL6 according to the manufacturer's instructions (R&D Systems, cat. DY406, DY410, DY411). Three biological samples per

510 condition were tested in technical duplicate, and experiments were repeated at least two times per
511 experimental condition.
512
513 **FluoroDOT assay**
514 Assays were performed using reagents from Mouse TNF-α DuoSet ELISA kits (R&D systems, catalog
515 number DY410-05). Wells of 96 well glass-bottom, black plates (P96-1.5H-N, Cellvis, Mountain View,
516 USA) were coated with 100μL TNF-α capture antibody (2 μg/mL in PBS) at 4°C overnight. Coated wells
517 were then washed 3 times with PBS, followed by blocking with reagent diluent (0.2μm filtered 1% BSA
518 in PBS) for at least 1 h at RT. Wells were washed 3 times with PBS and thereafter 8.0 x 10^3 BMDMs in
519 DMEM complete with 10% L cell supernatant were added to each well. The same day, BMDMs were
520 infected with the indicated GFP-expressing Mtb strains that had prepared as single cell suspensions.
521 Macrophages were incubated at 37°C in 5% CO_2 for 3 h, followed by 3 washes with fresh media to
522 remove extracellular Mtb, and incubated in the same media for an additional 3 h. Media was then
523 aspirated and 200μL 4% PFA in PBS was added for 30 min at 37°C. Wells were washed with PBS and
524 incubated with biotinylated 75 ng/mL TNF-α detection antibody in reagent diluent for 2 h at RT. Wells
525 were washed 3 times with PBS followed by 100μL PBS containing streptavidin plasmonic-fluor 650
526 (PF650, extinction 0.5; Auragent Bioscience LLC) (Wang et al., 2021) for 30 min at RT in the dark. Cells
527 were washed 3 times with PBS and stained with 300nM DAPI (Millipore Sigma) for 5 min at RT in the
528 dark. Wells were washed 3 times with PBS and then visualized using a Nikon TsR2 epifluorescence
529 microscope.
530
531 **Aerosol infection of mice**
532 Mtb was grown to mid-log phase (OD_{600} 0.5-0.8), centrifuged at 3000 x g, washed with PBS, and
533 resuspended in sterile water with 0.05% Tween-80. Single cell suspensions were generated using the
534 methods described above. Suspensions were diluted in sterile water with 0.05% Tween-80 to achieve
535 a final concentration of 1 x 10^5 bacteria/mL for the sp and so/sp preparations, and 2 x 10^5 bacteria/mL

for the 5μmF preparation, which yielded an inoculum of approximately 100 CFU. 5 mL of the bacterial suspension was aerosolized using a Glas-Col inhalation exposure system as previously described (Wolf et al., 2007). Three male and three female, total six mice were used in each group. The initial bacterial burden was confirmed by plating lung homogenates on 7H11 + 10% OADC on the day following infection. At the indicated time points, mice were euthanized with CO_2. Following euthanasia, lungs and spleens were extracted using aseptic technique and placed in 2 mL PBS. Lungs and spleens were homogenized, and serial dilutions were plated on 7H11 Middlebrook agar. In most of the experiments, the left lung was excised, placed in RNAlater (Invitrogen, AM7020), stored at 80°C, followed by RNA extraction using TRIzol as described above, while the right lung was homogenized in PBS and processed for CFU. CFU were enumerated 14 to 21 days after plating.

Transmission electron microscopy

Bacteria were grown to mid-log phase, and single cell suspensions were generated in PBS as described above. Bacteria were incubated in 4% PFA for 30 min at 37°C followed by centrifugation at 3000 x g and resuspension in PBS. For ultrastructural analyses using ultrathin cross-sections through bacteria, samples were further fixed in 2% paraformaldehyde/2.5% glutaraldehyde (Ted Pella Inc., Redding, CA) in 100 mM sodium cacodylate buffer, pH 7.2 for 2h at RT and then overnight at 4°C. Samples were washed in sodium cacodylate buffer at RT and postfixed in 2% osmium tetroxide (Ted Pella Inc) for 1h at RT. Samples were then rinsed in dH20, dehydrated in a graded series of ethanol, and embedded in Eponate 12 resin (Ted Pella Inc). Sections of 95 nm were cut with a Leica Ultracut UCT ultramicrotome (Leica Microsystems Inc., Bannockburn, IL), stained with uranyl acetate and lead citrate, and viewed on a JEOL 1200 EX transmission electron microscope (JEOL USA Inc., Peabody, MA) equipped with an AMT 8-megapixel digital camera and AMT Image Capture Engine V602 software (Advanced Microscopy Techniques, Woburn, MA).

For analyses of whole bacteria, after bacterial samples were fixed with 4% PFA, they were allowed to adsorb onto freshly glow discharged formvar/carbon-coated copper grids for 10 min. Grids were then

563 washed in dH2O and stained with 1% aqueous uranyl acetate (Ted Pella Inc.) for 1 min. Excess liquid
564 was gently wicked off, and grids were allowed to air dry. Samples were viewed by transmission electron
565 microscopy as described above.
566
567 **Methodology of literature review**
568 We conducted a search in PubMed using the medical subject headings "*Mycobacterium tuberculosis*"
569 and "Macrophage" and filtered for articles published in 2021. This generated 183 articles, which were
570 further filtered to include only original research articles by removing review articles, protocols, and
571 commentaries. The remaining 155 articles were included in the analysis if they performed an *in vitro*
572 macrophage infection with live Mtb. The text, supplementary methods, and figures were reviewed to
573 determine the single cell preparation methods used.
574
575 **Statistical analysis**
576 Graph Pad Prism 9 software was used for statistical analysis and to prepare graphs. Error bars used in
577 the figures correspond to the mean and standard deviation. Statistical significance was determined
578 using unpaired T test, one-way analysis of variance (ANOVA), or two-way ANOVA, as indicated.
579
580 **Acknowledgements**
581 We thank members of the Philips laboratory for their input. Funding for these studies came from
582 NIAID/NIH (R01 AI087682 and AI30454) to JAP, and the National Cancer Institute (NCI)-Innovative
583 Molecular Analysis Technologies (R21CA236652) and National Science Foundation (CBET-1900277)
584 to SS. ATR was supported by NIH/NHLBI (T32 HL007317-37). We thank the Genome Technology
585 Access Center at Washington University School of Medicine for help with genomic analysis. The Center
586 is partially supported by NCI Cancer Center Support Grant #P30 CA91842 to the Siteman Cancer
587 Center and by ICTS/CTSA Grant# UL1TR002345 from the National Center for Research
588 Resources (NCRR), a component of the National Institutes of Health (NIH), and NIH Roadmap

for Medical Research. This publication is solely the responsibility of the authors and does not necessarily represent the official view of NCRR or NIH.

Data availability

RNA-seq data will be deposited in a repository and made available.

Competing interests

SS is an inventor on a provisional patent related to plasmonic-fluor technology, and the technology has been licensed by the Office of Technology Management at Washington University in St. Louis to Auragent Bioscience LLC. SS is a co-founder/shareholder of Auragent Bioscience LLC. SS along with Washington University may have financial gain through Auragent Bioscience LLC through this licensing agreement. AS is currently employed with Auragent Bioscience LLC. These potential conflicts of interest have been disclosed and are being managed by Washington University in St. Louis.

Author contributions

The project was conceptualized by EM and JAP. All experiments were performed by EM and AR, and formal analysis was performed by AR, EM, and JAP. AS performed FluroDOT experiments. SS supervised FluroDOT studies. WB performed electron microscopy experiments. Funding was acquired by JAP and SS. Writing of the original draft was done by AR, EM, and JAP. Editing of the manuscript was done by all authors. JAP supervised the studies. EM and AR share the first author position, reflecting their equivalent contributions.

References

Astarie-Dequeker, C., Le Guyader, L., Malaga, W., Seaphanh, F. K., Chalut, C., Lopez, A., & Guilhot, C. (2009). Phthiocerol dimycocerosates of M. tuberculosis participate in macrophage invasion

616 by inducing changes in the organization of plasma membrane lipids. *PLoS Pathog*, *5*(2),
617 e1000289. https://doi.org/10.1371/journal.ppat.1000289

618 Athman, J. J., Wang, Y., McDonald, D. J., Boom, W. H., Harding, C. V., & Wearsch, P. A. (2015).
619 Bacterial Membrane Vesicles Mediate the Release of Mycobacterium tuberculosis Lipoglycans
620 and Lipoproteins from Infected Macrophages. *J Immunol*, *195*(3), 1044-1053.
621 https://doi.org/10.4049/jimmunol.1402894

622 Augenstreich, J., Arbues, A., Simeone, R., Haanappel, E., Wegener, A., Sayes, F., Le Chevalier, F.,
623 Chalut, C., Malaga, W., Guilhot, C., Brosch, R., & Astarie-Dequeker, C. (2017). ESX-1 and
624 phthiocerol dimycocerosates of Mycobacterium tuberculosis act in concert to cause
625 phagosomal rupture and host cell apoptosis. *Cell Microbiol*, *19*(7).
626 https://doi.org/10.1111/cmi.12726

627 Banaiee, N., Kincaid, E. Z., Buchwald, U., Jacobs, W. R., Jr., & Ernst, J. D. (2006). Potent inhibition of
628 macrophage responses to IFN-gamma by live virulent Mycobacterium tuberculosis is
629 independent of mature mycobacterial lipoproteins but dependent on TLR2. *J Immunol*, *176*(5),
630 3019-3027. https://doi.org/10.4049/jimmunol.176.5.3019

631 Barczak, A. K., Avraham, R., Singh, S., Luo, S. S., Zhang, W. R., Bray, M. A., Hinman, A. E.,
632 Thompson, M., Nietupski, R. M., Golas, A., Montgomery, P., Fitzgerald, M., Smith, R. S.,
633 White, D. W., Tischler, A. D., Carpenter, A. E., & Hung, D. T. (2017). Systematic,
634 multiparametric analysis of Mycobacterium tuberculosis intracellular infection offers insight into
635 coordinated virulence. *PLoS Pathog*, *13*(5), e1006363.
636 https://doi.org/10.1371/journal.ppat.1006363

637 Blanc, L., Gilleron, M., Prandi, J., Song, O. R., Jang, M. S., Gicquel, B., Drocourt, D., Neyrolles, O.,
638 Brodin, P., Tiraby, G., Vercellone, A., & Nigou, J. (2017). Mycobacterium tuberculosis inhibits

639 human innate immune responses via the production of TLR2 antagonist glycolipids. *Proc Natl*
640 *Acad Sci U S A*, *114*(42), 11205-11210. https://doi.org/10.1073/pnas.1707840114

641 Camacho, L. R., Constant, P., Raynaud, C., Laneelle, M. A., Triccas, J. A., Gicquel, B., Daffe, M., &
642 Guilhot, C. (2001). Analysis of the phthiocerol dimycocerosate locus of Mycobacterium
643 tuberculosis. Evidence that this lipid is involved in the cell wall permeability barrier. *J Biol*
644 *Chem*, *276*(23), 19845-19854. https://doi.org/10.1074/jbc.M100662200

645 Cambier, C. J., Banik, S. M., Buonomo, J. A., & Bertozzi, C. R. (2020). Spreading of a mycobacterial
646 cell-surface lipid into host epithelial membranes promotes infectivity. *Elife*, *9*.
647 https://doi.org/10.7554/eLife.60648

648 Cambier, C. J., Takaki, K. K., Larson, R. P., Hernandez, R. E., Tobin, D. M., Urdahl, K. B., Cosma, C.
649 L., & Ramakrishnan, L. (2014). Mycobacteria manipulate macrophage recruitment through
650 coordinated use of membrane lipids. *Nature*, *505*(7482), 218-222.
651 https://doi.org/10.1038/nature12799

652 Cheng, N., Porter, M. A., Frick, L. W., Nguyen, Y., Hayden, J. D., Young, E. F., Braunstein, M. S.,
653 Hull-Ryde, E. A., & Janzen, W. P. (2014). Filtration improves the performance of a high-
654 throughput screen for anti-mycobacterial compounds. *PLoS One*, *9*(5), e96348.
655 https://doi.org/10.1371/journal.pone.0096348

656 Cohen, S. B., Gern, B. H., Delahaye, J. L., Adams, K. N., Plumlee, C. R., Winkler, J. K., Sherman, D.
657 R., Gerner, M. Y., & Urdahl, K. B. (2018). Alveolar Macrophages Provide an Early
658 Mycobacterium tuberculosis Niche and Initiate Dissemination. *Cell Host Microbe*, *24*(3), 439-
659 446.e434. https://doi.org/10.1016/j.chom.2018.08.001

660 Cox, J. S., Chen, B., McNeil, M., & Jacobs, W. R., Jr. (1999). Complex lipid determines tissue-specific
661 replication of Mycobacterium tuberculosis in mice. *Nature*, *402*(6757), 79-83.

662 Dinkele, R., Gessner, S., McKerry, A., Leonard, B., Seldon, R., Koch, A. S., Morrow, C., Gqada, M.,
663 Kamariza, M., Bertozzi, C. R., Smith, B., McLoud, C., Kamholz, A., Bryden, W., Call, C.,
664 Kaplan, G., Mizrahi, V., Wood, R., & Warner, D. F. (2021). Capture and visualization of live
665 Mycobacterium tuberculosis bacilli from tuberculosis patient bioaerosols. *PLoS Pathog*, *17*(2),
666 e1009262. https://doi.org/10.1371/journal.ppat.1009262

667 Dulberger, C. L., Rubin, E. J., & Boutte, C. C. (2020). The mycobacterial cell envelope - a moving
668 target. *Nat Rev Microbiol*, *18*(1), 47-59. https://doi.org/10.1038/s41579-019-0273-7

669 Garcia-Vilanova, A., Chan, J., & Torrelles, J. B. (2019). Underestimated Manipulative Roles
670 of M*ycobacterium tuberculosis* Cell Envelope Glycolipids During Infection. *Front Immunol*, *10*,
671 2909. https://doi.org/10.3389/fimmu.2019.02909

672 Hinman, A. E., Jani, C., Pringle, S. C., Zhang, W. R., Jain, N., Martinot, A. J., & Barczak, A. K. (2021).
673 Mycobacterium tuberculosis canonical virulence factors interfere with a late component of the
674 TLR2 response. *Elife*, *10*. https://doi.org/10.7554/eLife.73984

675 Huang, L., Nazarova, E. V., Tan, S., Liu, Y., & Russell, D. G. (2018). Growth of Mycobacterium
676 tuberculosis in vivo segregates with host macrophage metabolism and ontogeny. *J Exp Med*,
677 *215*(4), 1135-1152. https://doi.org/10.1084/jem.20172020

678 Kalscheuer, R., Palacios, A., Anso, I., Cifuente, J., Anguita, J., Jacobs, W. R., Guerin, M. E., &
679 Prados-Rosales, R. (2019). The *Mycobacterium tuberculosis* capsule: a cell structure with key
680 implications in pathogenesis. *Biochem J*, *476*(14), 1995-2016.
681 https://doi.org/10.1042/BCJ20190324

682 Kolloli, A., Kumar, R., Singh, P., Narang, A., Kaplan, G., Sigal, A., & Subbian, S. (2021). Aggregation
683 state of Mycobacterium tuberculosis impacts host immunity and augments pulmonary disease
684 pathology. *Commun Biol*, *4*(1), 1256. https://doi.org/10.1038/s42003-021-02769-9

685 Lavalett, L., Rodriguez, H., Ortega, H., Sadee, W., Schlesinger, L. S., & Barrera, L. F. (2017). Alveolar
686 macrophages from tuberculosis patients display an altered inflammatory gene expression
687 profile. *Tuberculosis (Edinb)*, *107*, 156-167. https://doi.org/10.1016/j.tube.2017.08.012

688 Lemassu, A., & Daffe, M. (1994). Structural features of the exocellular polysaccharides of
689 Mycobacterium tuberculosis. *Biochem J*, *297 (Pt 2)*, 351-357.
690 https://doi.org/10.1042/bj2970351

691 Lemassu, A., Ortalo-Magne, A., Bardou, F., Silve, G., Laneelle, M. A., & Daffe, M. (1996).
692 Extracellular and surface-exposed polysaccharides of non-tuberculous mycobacteria.
693 *Microbiology (Reading)*, *142 (Pt 6)*, 1513-1520. https://doi.org/10.1099/13500872-142-6-1513

694 Lerner, T. R., Queval, C. J., Fearns, A., Repnik, U., Griffiths, G., & Gutierrez, M. G. (2018).
695 Phthiocerol dimycocerosates promote access to the cytosol and intracellular burden of
696 Mycobacterium tuberculosis in lymphatic endothelial cells. *BMC Biol*, *16*(1), 1.
697 https://doi.org/10.1186/s12915-017-0471-6

698 Liang, C., Luan, J., Wang, Z., Jiang, Q., Gupta, R., Cao, S., Liu, K. K., Morrissey, J. J., Kharasch, E.
699 D., Naik, R. R., & Singamaneni, S. (2021). Gold Nanorod Size-Dependent Fluorescence
700 Enhancement for Ultrasensitive Fluoroimmunoassays. *ACS Appl Mater Interfaces*, *13*(9),
701 11414-11423. https://doi.org/10.1021/acsami.0c20303

702 Liberzon, A., Birger, C., Thorvaldsdottir, H., Ghandi, M., Mesirov, J. P., & Tamayo, P. (2015). The
703 Molecular Signatures Database (MSigDB) hallmark gene set collection. *Cell Syst*, *1*(6), 417-
704 425. https://doi.org/10.1016/j.cels.2015.12.004

705 Mahamed, D., Boulle, M., Ganga, Y., Mc Arthur, C., Skroch, S., Oom, L., Catinas, O., Pillay, K.,
706 Naicker, M., Rampersad, S., Mathonsi, C., Hunter, J., Wong, E. B., Suleman, M., Sreejit, G.,
707 Pym, A. S., Lustig, G., & Sigal, A. (2017). Intracellular growth of Mycobacterium tuberculosis

after macrophage cell death leads to serial killing of host cells. *Elife*, *6*. https://doi.org/10.7554/eLife.22028

Murry, J. P., Pandey, A. K., Sassetti, C. M., & Rubin, E. J. (2009). Phthiocerol dimycocerosate transport is required for resisting interferon-gamma-independent immunity. *J Infect Dis*, *200*(5), 774-782. https://doi.org/10.1086/605128

Ortalo-Magne, A., Dupont, M. A., Lemassu, A., Andersen, A. B., Gounon, P., & Daffe, M. (1995). Molecular composition of the outermost capsular material of the tubercle bacillus. *Microbiology (Reading)*, *141 (Pt 7)*, 1609-1620. https://doi.org/10.1099/13500872-141-7-1609

Osman, M. M., Pagán, A. J., Shanahan, J. K., & Ramakrishnan, L. (2020). Mycobacterium marinum phthiocerol dimycocerosates enhance macrophage phagosomal permeabilization and membrane damage. *PLoS One*, *15*(7), e0233252. https://doi.org/10.1371/journal.pone.0233252

Palacios, A., Gupta, S., Rodriguez, G. M., & Prados-Rosales, R. (2021). Extracellular vesicles in the context of Mycobacterium tuberculosis infection. *Mol Immunol*, *133*, 175-181. https://doi.org/10.1016/j.molimm.2021.02.010

Pisu, D., Huang, L., Grenier, J. K., & Russell, D. G. (2020). Dual RNA-Seq of Mtb-Infected Macrophages In Vivo Reveals Ontologically Distinct Host-Pathogen Interactions. *Cell Rep*, *30*(2), 335-350.e334. https://doi.org/10.1016/j.celrep.2019.12.033

Prados-Rosales, R., Baena, A., Martinez, L. R., Luque-Garcia, J., Kalscheuer, R., Veeraraghavan, U., Camara, C., Nosanchuk, J. D., Besra, G. S., Chen, B., Jimenez, J., Glatman-Freedman, A., Jacobs, W. R., Jr., Porcelli, S. A., & Casadevall, A. (2011). Mycobacteria release active membrane vesicles that modulate immune responses in a TLR2-dependent manner in mice. *J Clin Invest*, *121*(4), 1471-1483. https://doi.org/10.1172/JCI44261

731 Prados-Rosales, R., Carreno, L. J., Weinrick, B., Batista-Gonzalez, A., Glatman-Freedman, A., Xu, J.,
732 Chan, J., Jacobs, W. R., Jr., Porcelli, S. A., & Casadevall, A. (2016). The Type of Growth
733 Medium Affects the Presence of a Mycobacterial Capsule and Is Associated With Differences
734 in Protective Efficacy of BCG Vaccination Against Mycobacterium tuberculosis. *J Infect Dis*,
735 *214*(3), 426-437. https://doi.org/10.1093/infdis/jiw153

736 Quigley, J., Hughitt, V. K., Velikovsky, C. A., Mariuzza, R. A., El-Sayed, N. M., & Briken, V. (2017).
737 The Cell Wall Lipid PDIM Contributes to Phagosomal Escape and Host Cell Exit of
738 Mycobacterium tuberculosis. *mBio*, *8*(2). https://doi.org/10.1128/mBio.00148-17

739 Reed, M. B., Domenech, P., Manca, C., Su, H., Barczak, A. K., Kreiswirth, B. N., Kaplan, G., & Barry,
740 C. E. (2004). A glycolipid of hypervirulent tuberculosis strains that inhibits the innate immune
741 response. *Nature*, *431*(7004), 84-87. https://doi.org/10.1038/nature02837

742 Rodel, H. E., Ferreira, I., Ziegler, C. G. K., Ganga, Y., Bernstein, M., Hwa, S. H., Nargan, K., Lustig,
743 G., Kaplan, G., Noursadeghi, M., Shalek, A. K., Steyn, A. J. C., & Sigal, A. (2021). Aggregated
744 Mycobacterium tuberculosis Enhances the Inflammatory Response. *Front Microbiol*, *12*,
745 757134. https://doi.org/10.3389/fmicb.2021.757134

746 Rothchild, A. C., Olson, G. S., Nemeth, J., Amon, L. M., Mai, D., Gold, E. S., Diercks, A. H., &
747 Aderem, A. (2019). Alveolar macrophages generate a noncanonical NRF2-driven
748 transcriptional response to Mycobacterium tuberculosis in vivo. *Sci Immunol*, *4*(37).
749 https://doi.org/10.1126/sciimmunol.aaw6693

750 Rousseau, C., Winter, N., Pivert, E., Bordat, Y., Neyrolles, O., Ave, P., Huerre, M., Gicquel, B., &
751 Jackson, M. (2004). Production of phthiocerol dimycocerosates protects Mycobacterium
752 tuberculosis from the cidal activity of reactive nitrogen intermediates produced by
753 macrophages and modulates the early immune response to infection. *Cell Microbiol*, *6*(3), 277-
754 287. https://doi.org/10.1046/j.1462-5822.2004.00368.x

Sani, M., Houben, E. N., Geurtsen, J., Pierson, J., de Punder, K., van Zon, M., Wever, B., Piersma, S. R., Jimenez, C. R., Daffe, M., Appelmelk, B. J., Bitter, W., van der Wel, N., & Peters, P. J. (2010). Direct visualization by cryo-EM of the mycobacterial capsular layer: a labile structure containing ESX-1-secreted proteins. *PLoS Pathog*, *6*(3), e1000794. https://doi.org/10.1371/journal.ppat.1000794

Siméone, R., Constant, P., Malaga, W., Guilhot, C., Daffé, M., & Chalut, C. (2007). Molecular dissection of the biosynthetic relationship between phthiocerol and phthiodiolone dimycocerosates and their critical role in the virulence and permeability of Mycobacterium tuberculosis. *FEBS J*, *274*(8), 1957-1969. https://doi.org/10.1111/j.1742-4658.2007.05740.x

Stokes, R. W., Norris-Jones, R., Brooks, D. E., Beveridge, T. J., Doxsee, D., & Thorson, L. M. (2004). The glycan-rich outer layer of the cell wall of Mycobacterium tuberculosis acts as an antiphagocytic capsule limiting the association of the bacterium with macrophages. *Infect Immun*, *72*(10), 5676-5686. https://doi.org/10.1128/IAI.72.10.5676-5686.2004

Stukalov, O., Korenevsky, A., Beveridge, T. J., & Dutcher, J. R. (2008). Use of atomic force microscopy and transmission electron microscopy for correlative studies of bacterial capsules. *Appl Environ Microbiol*, *74*(17), 5457-5465. https://doi.org/10.1128/AEM.02075-07

Subramanian, A., Tamayo, P., Mootha, V. K., Mukherjee, S., Ebert, B. L., Gillette, M. A., Paulovich, A., Pomeroy, S. L., Golub, T. R., Lander, E. S., & Mesirov, J. P. (2005). Gene set enrichment analysis: a knowledge-based approach for interpreting genome-wide expression profiles. *Proc Natl Acad Sci U S A*, *102*(43), 15545-15550. https://doi.org/10.1073/pnas.0506580102

Ufimtseva, E. G., Eremeeva, N. I., Petrunina, E. M., Umpeleva, T. V., Bayborodin, S. I., Vakhrusheva, D. V., & Skornyakov, S. N. (2018). Mycobacterium tuberculosis cording in alveolar macrophages of patients with pulmonary tuberculosis is likely associated with increased

mycobacterial virulence. *Tuberculosis (Edinb)*, *112*, 1-10. https://doi.org/10.1016/j.tube.2018.07.001

Vijay, S., Hai, H. T., Thu, D. D. A., Johnson, E., Pielach, A., Phu, N. H., Thwaites, G. E., & Thuong, N. T. T. (2017). Ultrastructural Analysis of Cell Envelope and Accumulation of Lipid Inclusions in Clinical Mycobacterium tuberculosis Isolates from Sputum, Oxidative Stress, and Iron Deficiency. *Front Microbiol*, *8*, 2681. https://doi.org/10.3389/fmicb.2017.02681

Wang, Z., Luan, J., Seth, A., Liu, L., You, M., Gupta, P., Rathi, P., Wang, Y., Cao, S., Jiang, Q., Zhang, X., Gupta, R., Zhou, Q., Morrissey, J. J., Scheller, E. L., Rudra, J. S., & Singamaneni, S. (2021). Microneedle patch for the ultrasensitive quantification of protein biomarkers in interstitial fluid. *Nat Biomed Eng*, *5*(1), 64-76. https://doi.org/10.1038/s41551-020-00672-y

Wells, W. F. (1946). A Method for Obtaining Standard Suspensions of Tubercle Bacilli in the Form of Single Cells. *Science*, *104*(2698), 254-255. https://doi.org/10.1126/science.104.2698.254

Wolf, A. J., Linas, B., Trevejo-Nunez, G. J., Kincaid, E., Tamura, T., Takatsu, K., & Ernst, J. D. (2007). Mycobacterium tuberculosis infects dendritic cells with high frequency and impairs their function in vivo. *J Immunol*, *179*(4), 2509-2519. https://doi.org/10.4049/jimmunol.179.4.2509

Figure 1

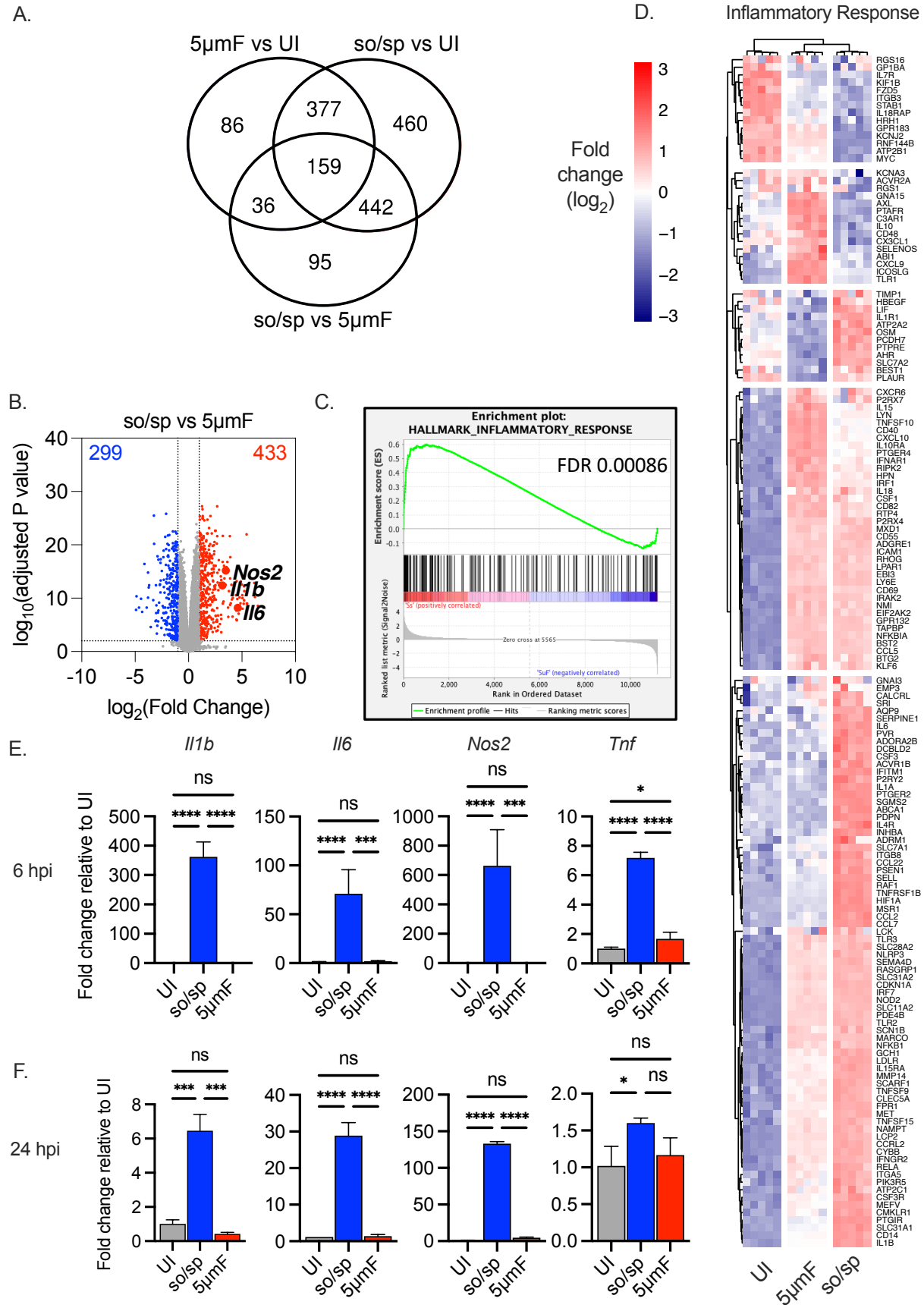

795

Figure 1. Cell preparation methods of Mtb impact macrophage responses

(**A-D**) BMDMs were uninfected or infected with Mtb prepared by sonication and spin (so/sp) or filtration (5μmF) at an MOI of 5 and analyzed 72 hpi by RNA-seq (n=5 per condition). **(A)** Venn diagram illustrates the number of DEGs between samples. **(B)** Volcano plot shows genes differentially expressed in BMDMs infected with so/sp versus 5μmF Mtb. DEGs exhibiting an adjusted P-value of ≤0.01 and a linear fold change ≥2.00 (red) or ≤2.00 (blue) are indicated. **(C-D)** GSEA identified hallmark gene sets that were significantly enriched in so/sp- versus 5μmF-infected BMDMs (P ≤0.01; FDR ≤0.01). Representative enrichment plot (C) and corresponding heat map (D) for the gene set "inflammatory response." Expression values in heatmap were generated using log2 normalized CPM for each gene. **(E and F)** qPCR was performed on uninfected BMDMs or BMDMs infected with so/sp- or 5μmF-prepared Mtb at 6 (E) and 24 (F) hpi using an MOI of 10. Data are shown as fold change in gene expression relative to uninfected BMDMs. Data shown are mean +/- SD from one representative experiment with 3 biological and 2 technical replicates for each group. qPCR experiments were performed at least 3 independent times. Statistical significance was determined with one-way ANOVA using Tukey's multiple comparisons test. (A-F) Error bars indicate mean +/- SD. ns not significant; *P<0.05; ***< 0.001; ****< 0.0001.

Figure 2

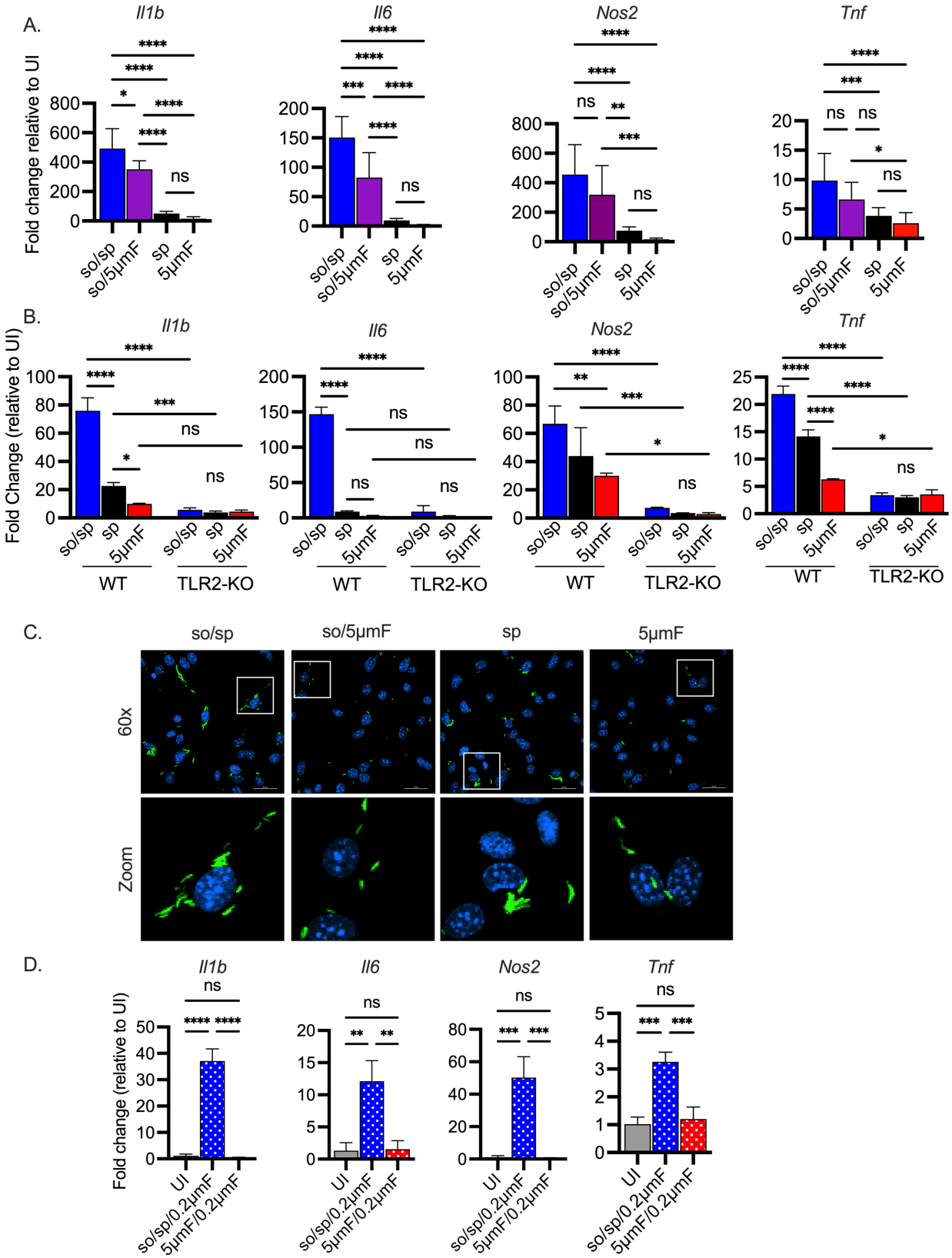

Figure 2. Sonicated bacteria induce high TLR2-dependent inflammatory responses

(A) BMDMs were uninfected or infected with different preparations of Mtb as indicated at an MOI of 10 and analyzed by qPCR 6 hpi. Data are presented as fold changes in gene expression relative to uninfected BMDMs. Data are combined from 2 to 3 experiments, each with 3 biological replicates in experimental duplicate. Statistical significance was determined with one-way ANOVA using Tukey's multiple comparisons test. qPCR data are presented as fold change in gene expression relative to uninfected BMDMs. **(B)** WT or *Tlr2*$^{-/-}$ BMDMs were uninfected or infected with different preparations of Mtb as indicated for 6 h at an MOI of 10 and analyzed by qPCR. Data are presented as fold change in gene expression relative to uninfected BMDMs of the same mouse genotype. Data are representative of 3 experiments, each with 3 biological replicates in experimental duplicate. Statistical significance was determined with two-way ANOVA using Tukey's multiple comparisons test. (**C**) Fluorescence microscopy images of GFP-expressing Mtb infected BMDMs. Nuclei were stained with DAPI. Images are maximum-intensity projections. Boxed areas in the merged image are shown in higher magnification in the bottom panel. (**D**) BMDMs were untreated or treated with the sterile filtrate from different preparations of Mtb for 6h and analyzed by qPCR. Data are presented as fold changes in gene expression relative to untreated BMDMs. Data are representative of 3 experiments, each with 3 biological replicates in experimental duplicate. Statistical significance was determined with one-way ANOVA using Tukey's multiple comparisons test. **(A-B, D)** Error bars indicate mean +/- SD. ns not significant; *P<0.05; **<0.01; ***< 0.001; ****< 0.0001.

Figure 3

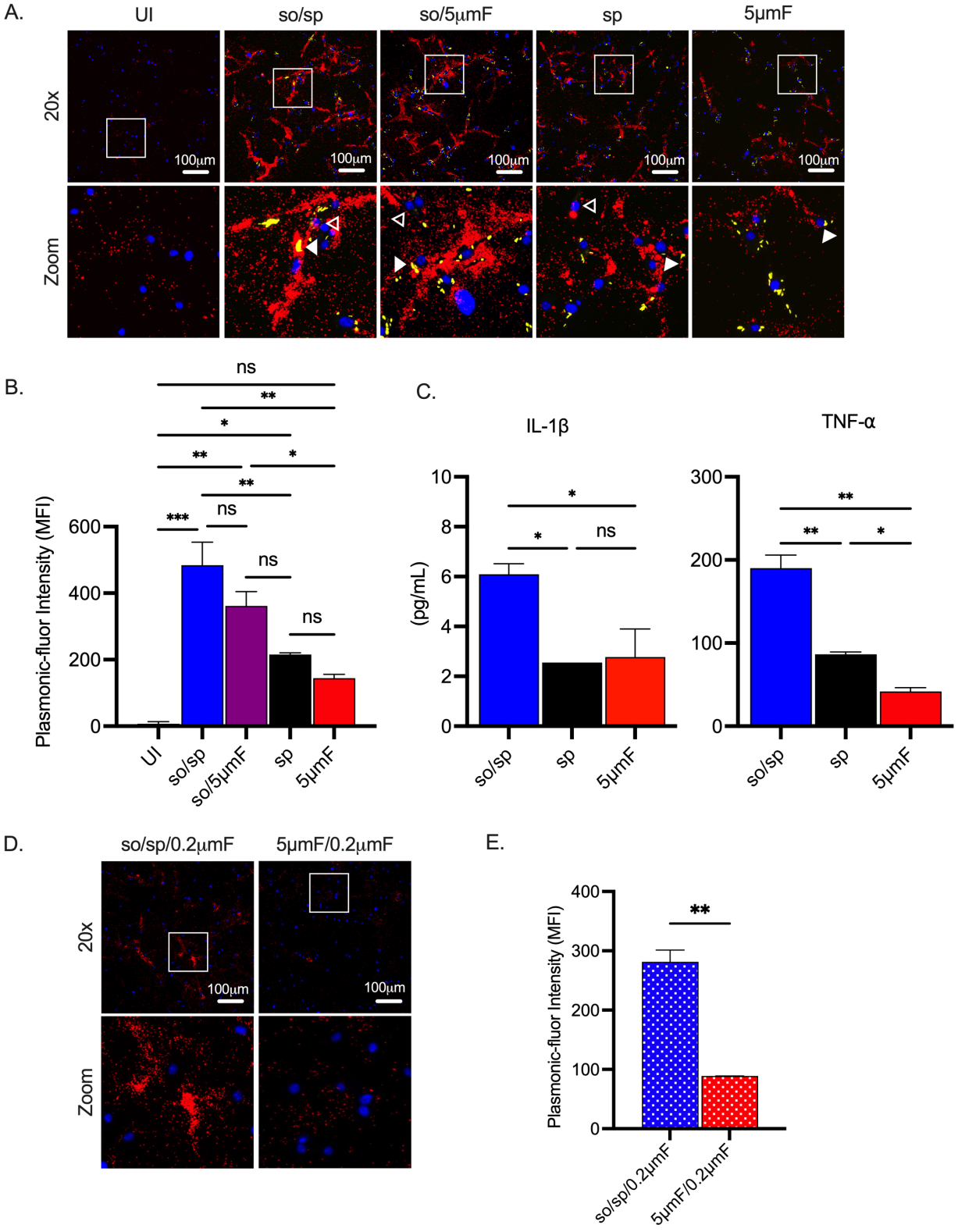

Figure 3. Sonicated bacteria elicit elevated TNF-α and IL-1β secretion

(A) Using the FluoroDOT assay, BMDMs were grown on a glass bottom plate that was coated with TNF-α capture antibody, infected at an MOI of 10 with H37Rv-GFP prepared by the indicated method, and examined by epifluorescence microscopy (20X) 6 hpi. Images show Plasmonic-fluor 650 (red), Mtb (GFP), and DAPI (blue). Boxed areas in the image are enlarged in the bottom images. Secretion from infected BMDMs or uninfected bystander cells are highlighted by open or closed white arrowheads, respectively. **(B)** Data show the quantification of the mean fluorescence intensity (MFI) of the plasmonic-fluor in the entire well from each different conditions shown in A with statistical significance determined with one-way ANOVA using Tukey's multiple comparisons test. **(C)** IL1-β and TNF-α were measured 24 hpi in the culture supernatant of uninfected or Mtb-infected BMDMs (MOI 10) by ELISA. Data shown are mean +/- SD from one representative experiment with 3 biological in experimental duplicate for each group. Significance was determined using one-way ANOVA with Tukeys' multiple comparisons test. **(D)** Using the FluoroDOT assay, BMDMs grown on a glass bottom plate that was coated with TNF-α capture antibody were exposed to the sterile filtrate of bacterial single cell suspension prepared by either so/sp or 5μmF and examined by epifluorescence microscopy (20X) 6 hpi. Images show Plasmonic-fluor 650 (red) and DAPI (blue). Boxed areas in the image are enlarged in the bottom images. **(E)** Data show the quantification of the mean fluorescence intensity (MFI) of the plasmonic-fluor in the entire well from each condition shown in D, with statistical significance determined using an unpaired T test. (A-E) Error bars indicate mean +/- SD. ns not significant; *P<0.05; **<0.01; ***<0.001.

Figure 4

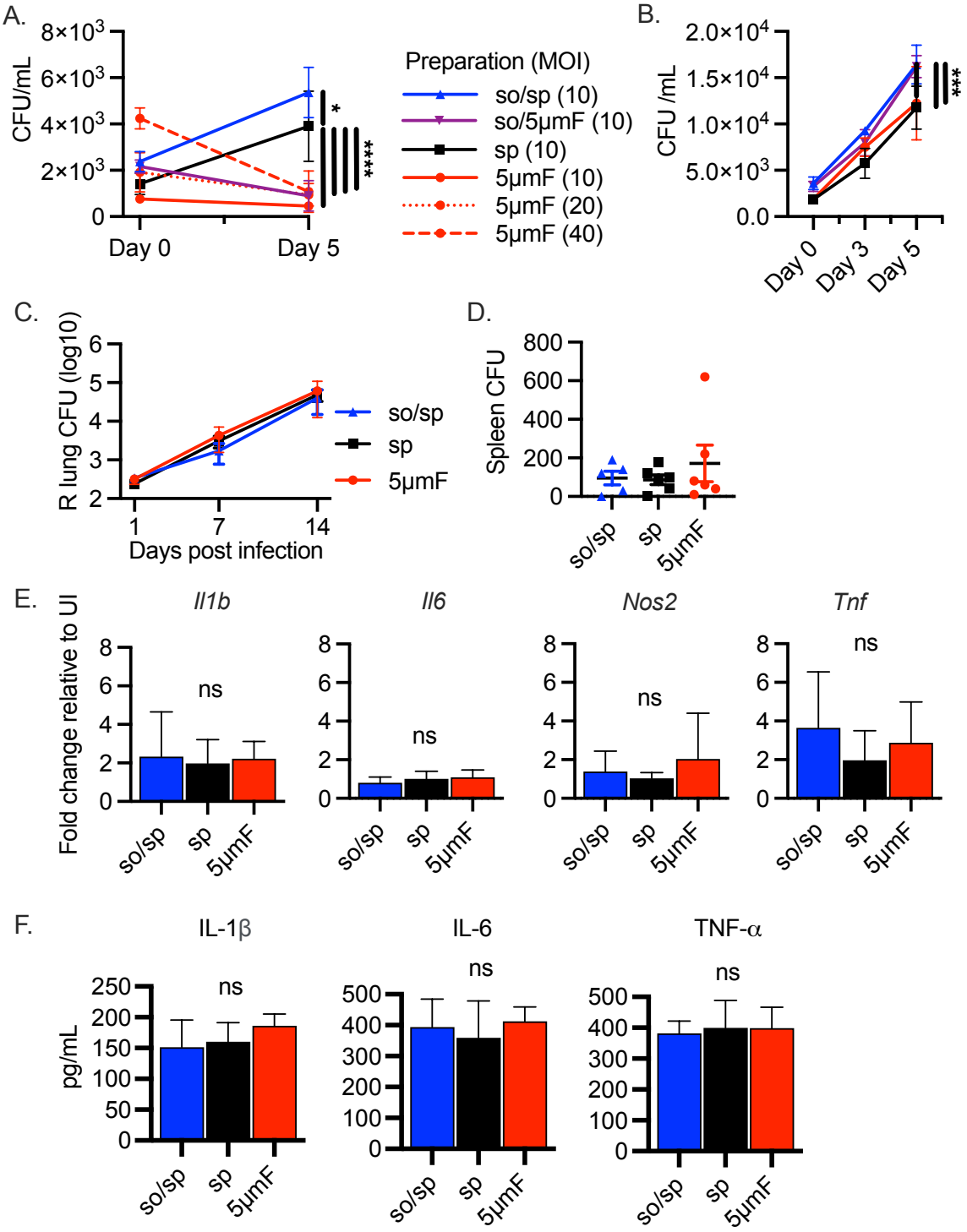

862

863 **Figure 4. Filtered Mtb are attenuated in BMDMs but not AMs or *in vivo***

864 **(A-B)** BMDMs (A) and alveolar macrophages (B) were infected with different preparations of Mtb at an

865 MOI of 10 and intracellular bacteria were enumerated by colony forming units (CFU) 4 hpi, 3 dpi, or 5

dpi. 5 biological replicates were used for each group in these experiments. Statistical significance between preparations was determined with two-way ANOVA using Tukey's multiple comparisons test with selected significance values presented for 5 dpi relative to spin preparation. (**C)** Right lung CFU at 1, 7, and 14 days following aerosol infection of Mtb with the indicated preparation method. Statistical significance between preparations was determined with two-way ANOVA using Tukey's multiple comparisons test. (**D)** Spleen CFU 14 days following aerosol infection of Mtb with the indicated preparation method. Statistical significance between preparations was determined with one-way ANOVA using Tukey's multiple comparisons test. **(E)** qPCR of right lung homogenate from lungs of infected mice at 14 dpi. Gene expression is presented as fold change relative to uninfected mice. 6 mice from each group were analyzed. Statistical significance between preparations was determined with one-way ANOVA using Tukey's multiple comparisons test. (**F**) Cytokine concentrations were determined using ELISA from homogenized left lungs of mice at 14 days following aerosol infection. 6 mice from each group were analyzed. Statistical significance between preparations was determined with one-way ANOVA using Tukey's multiple comparisons test. (**A-F**) Error bars indicate mean +/- SD. ns not significant; *P<0.05; **<0.01; ***<0.001; ****<0.0001.

Figure 5

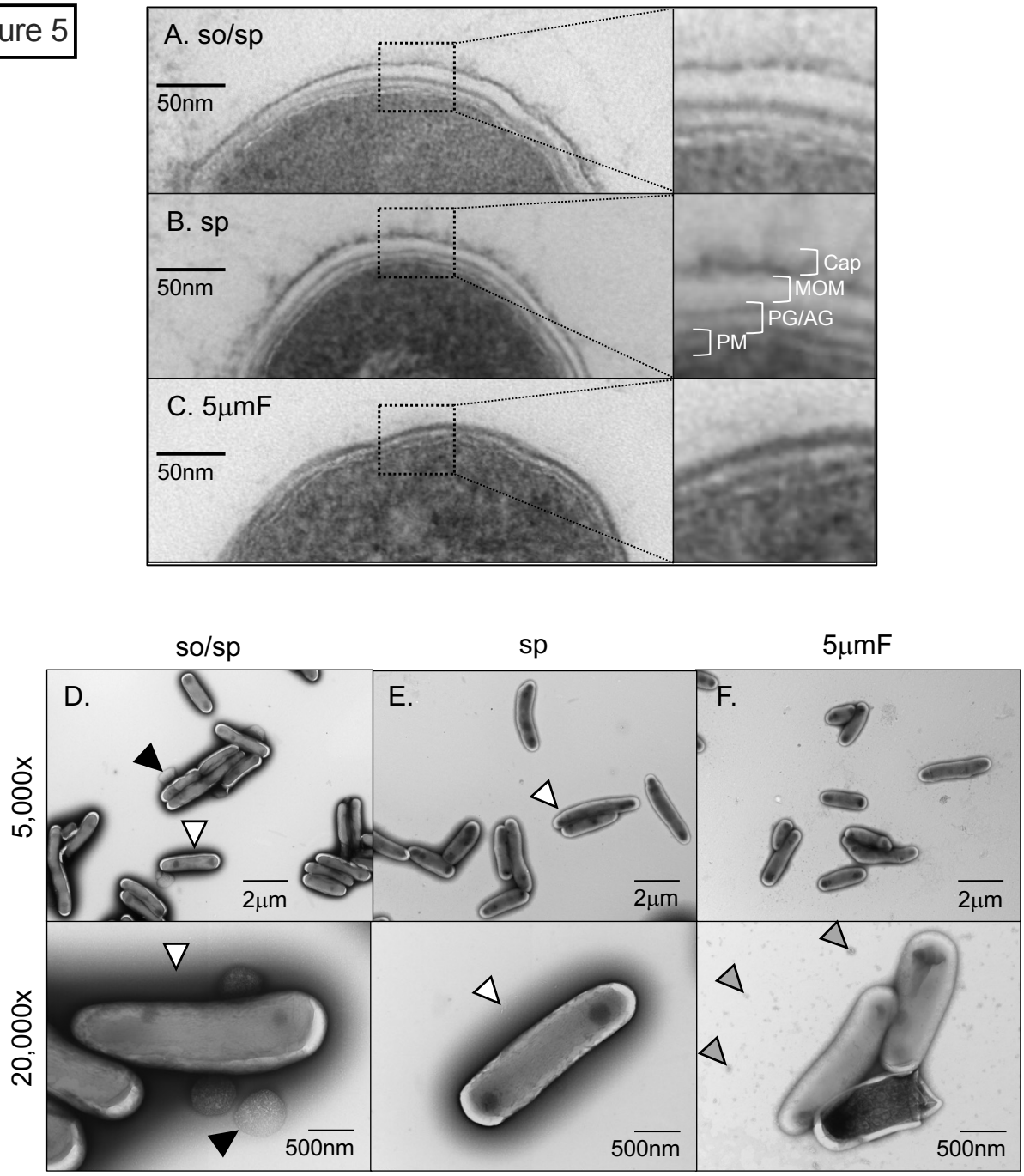

882

883

884 **Figure 5. Sonication and filtering affect the bacterial cell wall.**

885 **(A-C)** TEM of ultrathin cross-sections of Mtb at 50,000x magnification (left) beside enlarged cross-
886 section of the envelope (right). The plasma membrane (PM), peptidoglycan/arabinogalactan layer
887 (PG/AM), mycobacterial outer membrane (MOM), and capsular layer (Cap) are indicated. **(D-F)** Mtb
888 were absorbed on freshly glow discharged formvar/carbon-coated copper grids followed by negative

889 staining with 1% aqueous uranyl acetate. Representative images are 5,000x (above) and 20,000x
890 (below). So/sp-prepared Mtb had round protuberances that were on or near their envelopes indicated
891 by black arrows. Electron-dense outer halos seen surrounding so/sp- and sp-prepared bacteria are
892 indicated with white arrows. Debris seen in the extracellular space of 5μmF-prepared Mtb is indicated
893 with gray arrows.
894
895

Figure 6

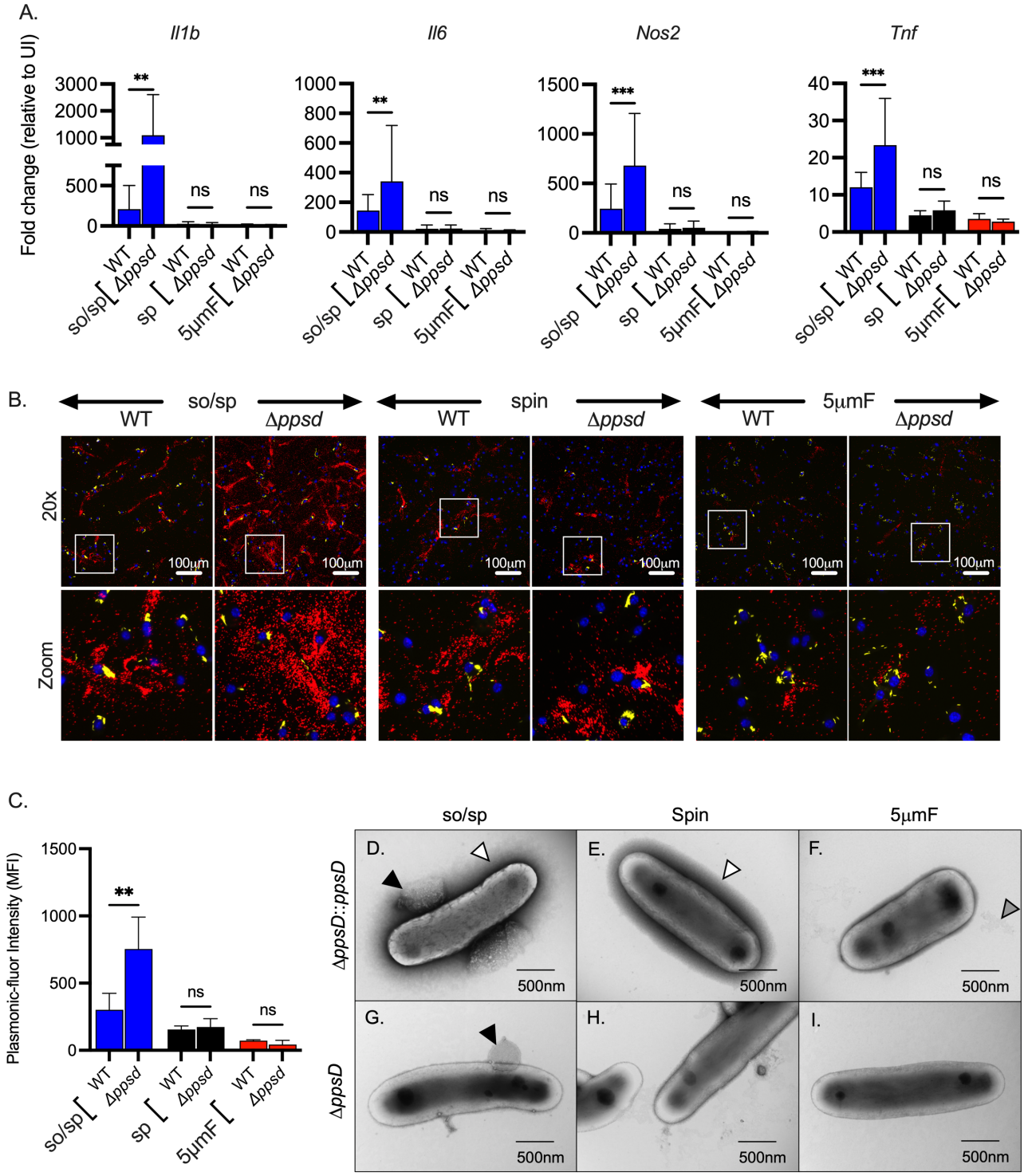

Figure 6. The role of PDIM in inflammatory responses depends upon preparation method

(A) BMDMs were uninfected or infected with indicated strains of Mtb at an MOI of 10, and gene expression was analyzed by qPCR at 6 hpi. Data are presented as fold change in gene expression relative to uninfected BMDMs of the same mouse genotype. Data are representative of 3 experiments, each with 3 biological replicates performed in experimental duplicate. Statistical significance was determined with two-way ANOVA using Tukey's multiple comparisons test. Data are combined from 2 to 3 experiments, each with 3 biological replicates performed in experimental duplicate. **(B)** Using the FluoroDOT assay, BMDMs were grown on a glass bottom plate that was coated with TNF-α capture antibody, infected at an MOI of 10 with H37Rv-GFP or Δ*ppsD*-GFP prepared by the indicated method, and examined by epifluorescence microscopy (20X) 6 hpi. Images show Plasmonic-fluor 650 (red), Mtb (GFP), and DAPI (blue). Boxed areas in the image are enlarged in the bottom images. **(C)** Data show the quantification of the mean fluorescence intensity (MFI) of the plasmonic-fluor in the entire well from each conditions shown in B with statistical significance determined with two-way ANOVA using Tukey's multiple comparisons test. **(D)** Bacteria were imaged by allowing indicated Mtb strains to absorb on freshly glow discharged formvar/carbon-coated copper grids followed by negative staining with 1% aqueous uranyl acetate. Round protuberances seen on or near the envelopes of so/sp-prepared H37Rv Mtb are indicated by black arrows, the electron-dense outer halos seen surrounding so/sp- and sp-prepared H37Rv Mtb are indicated with white arrows, and the debris seen in 5μmF-prepared H37Rv Mtb are indicated with gray arrows. **(A, C)** Error bars indicate mean +/- SD. ns not significant; **P<0.01; ***<0.001.

Supplementary Files

Supplemental Table 1. RNA-seq data

This file lists the genes that were differentially expressed between uninfected macrophages, macrophages infected with Mtb prepared by sonication followed by low-speed spin (so/sp), and macrophages infected with Mtb prepared by passing through a 5μm filter (5μmF). Infectious were carried out at an MOI of 5 at 72 hpi.

Supplemental Table 2. PCR primers used

Name	Primer
M. musculus Gapdh F	AGGTCGGTGTGAACGGATTTG
M. musculus Gapdh R	TGTAGACCATGTAGTTGAGGTCA
M. musculus Il1b F	GCAACTGTTCCTGAACTCAACT
M. musculus Il1b R	ATCTTTTGGGGTCCGTCAACT
M. musculus Il6 F	TAGTCCTTCCTACCCCAATTTCC
M. musculus Il6 R	TTGGTCCTTAGCCACTCCTTC
M. musculus Nos2 F	GTTCTCAGCCCAACAATACAA GA
M. musculus Nos2 R	GTGGACGGGTCGATGTCAC
M. musculus Tnf F	CCCTCACACTCAGATCATCTTCT
M. musculus Tnf R	GCTACGACGTGGGCTACAG

Figure S1

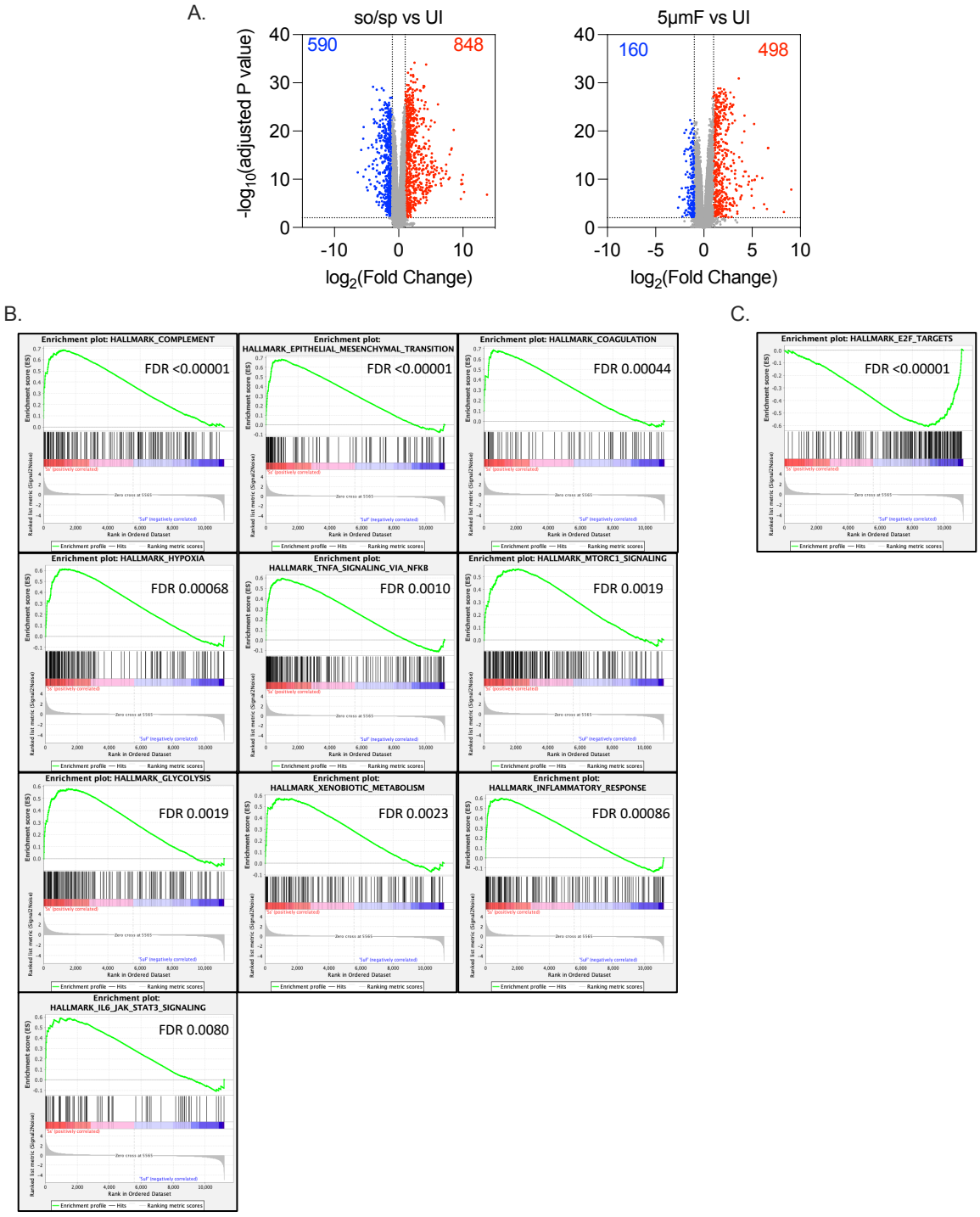

Supplemental Figure 1. Infection-induced changes in macrophage gene expression depend on whether Mtb are sonicated or filtered

(A) Volcano plot shows genes differentially expressed in BMDMs infected with so/sp versus UI (left) or 5μmF Mtb versus UI (right). DEGs exhibiting an adjusted P-value of ≤0.01 and a linear fold change ≥2.00 (red) or ≤2.00 (blue) are indicated. **(B-C)** Gene set enrichment analysis (GSEA) leading edge graphs of hallmark gene sets that were enriched in BMDMs infected with so/sp relative to 5μmF Mtb (B) or 5μmF relative to so/sp (C).

Figure S2

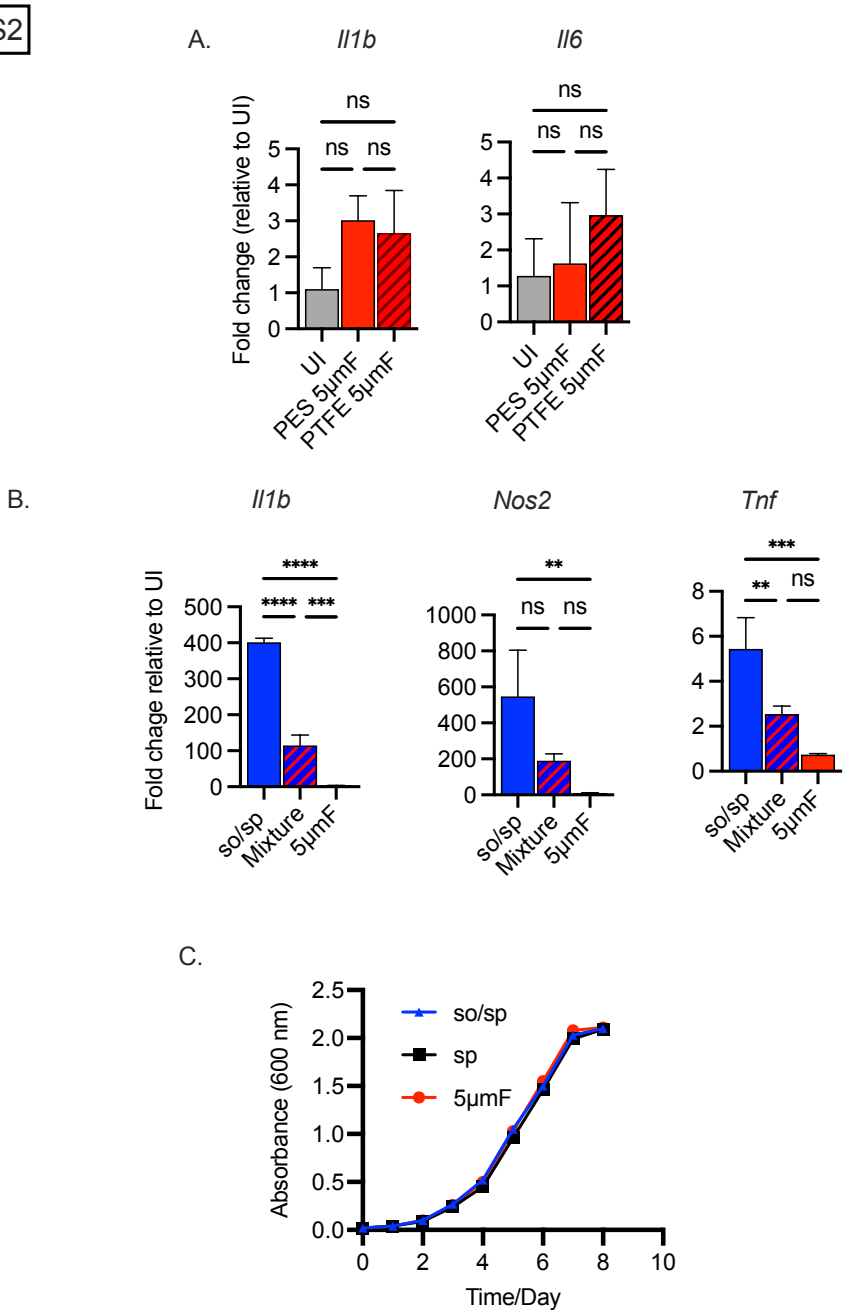

Supplemental Figure 2. Filtered Mtb are uninflammatory irrespective of filter type, do not strongly inhibit response from sonicated bacteria, and grow normally in vitro.
(A) BMDMs were uninfected or infected with Mtb prepared by passing through a 5μmF made of either PES or PTFE using a MOI of 10 and analyzed by qPCR 6 hpi. Data are presented as fold changes in gene expression relative to uninfected BMDMs. **(B)** BMDMs were uninfected or infected for 6h at a MOI of 10 with bacteria prepared by the so/sp or 5μmF-preparation or a mixture (1:1) of the two samples. Data are presented as fold change in gene expression relative to uninfected BMDMs. (**A-B**) Each group used 3 biological replicates performed in experimental duplicate. Statistical significance was determined with one-way ANOVA using Tukey's multiple comparisons test. qPCR data are presented as fold change in gene expression relative to uninfected BMDMs. Error bars indicate mean +/- SD. ns not significant; **P<0.01; ***<0.001; ****<0.0001. **(C)** Growth curve of different bacterial preparation in liquid media (7H9 media supplemented with 10% Middlebrook OADC, 0.05% Tyloxapol, and 0.2% glycerol).

Figure S3

A.

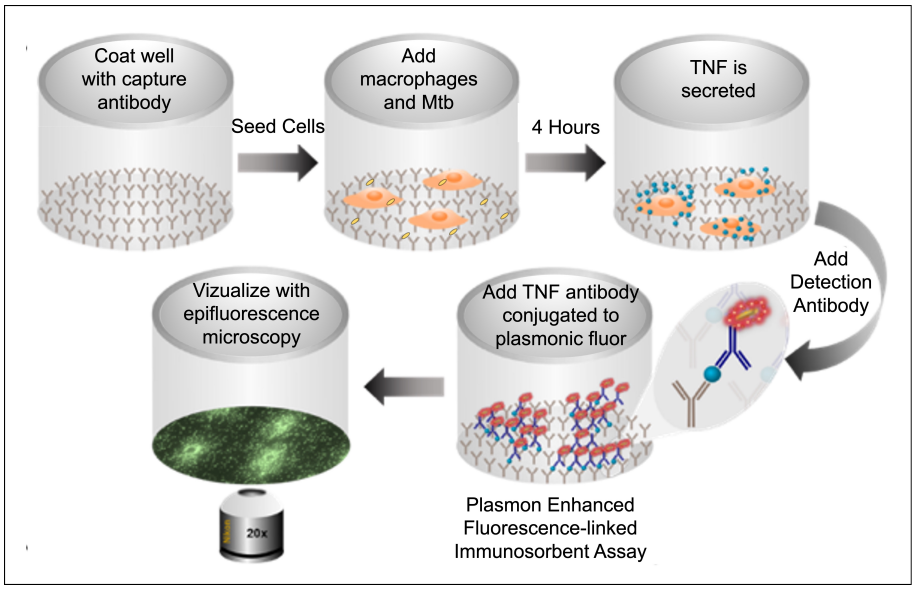

B.

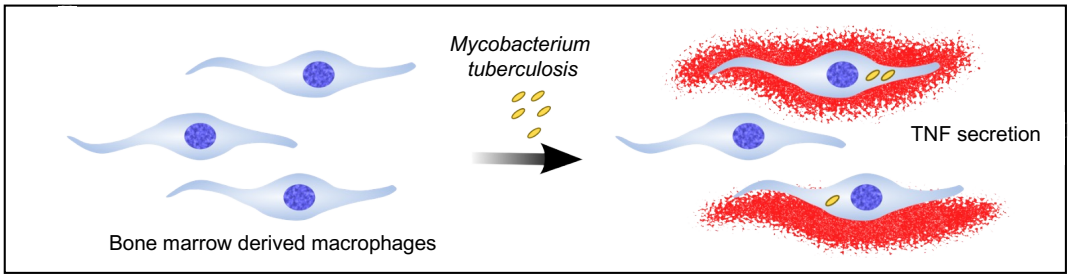

C.

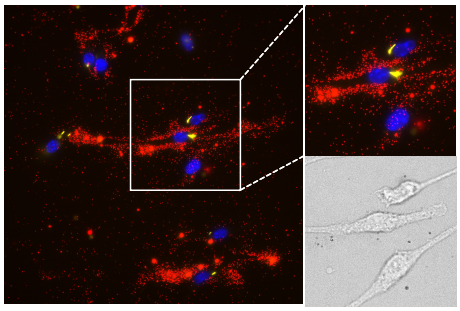

960
961
962 **Supplemental Figure 3. Schematic representation of the FluoroDOT assay**
963 **(A)** 96-well glass bottom plates are coated with TNF-α capture antibody, followed by the
964 addition of BMDMs. The macrophages are then infected with Mtb. TNF-α that is secreted by the
965 BMDMs can be bound by the capture antibody. Samples are fixed and then the detection
966 antibody, which is conjugated to plasmon-fluor 650, is added and the plate is visualized using
967 epifluorescence microscopy**. (B)** Illustration indicating how the assay can reveal TNF-α
968 secretion from Mtb-infected or bystander macrophages. (**C**) Representative fluorescent image
969 with zoomed region and corresponding brightfield image. The three cells in the images
970 demonstrate examples of an infected macrophage secreting substantial TNF-α (middle), an
971 infected cell with little TNF-α secretion (top), and an uninfected within minimal TNF-α secretion
972 (bottom). Macrophages were stained with DAPI (blue); TNF-α is red.

Figure S4

A.

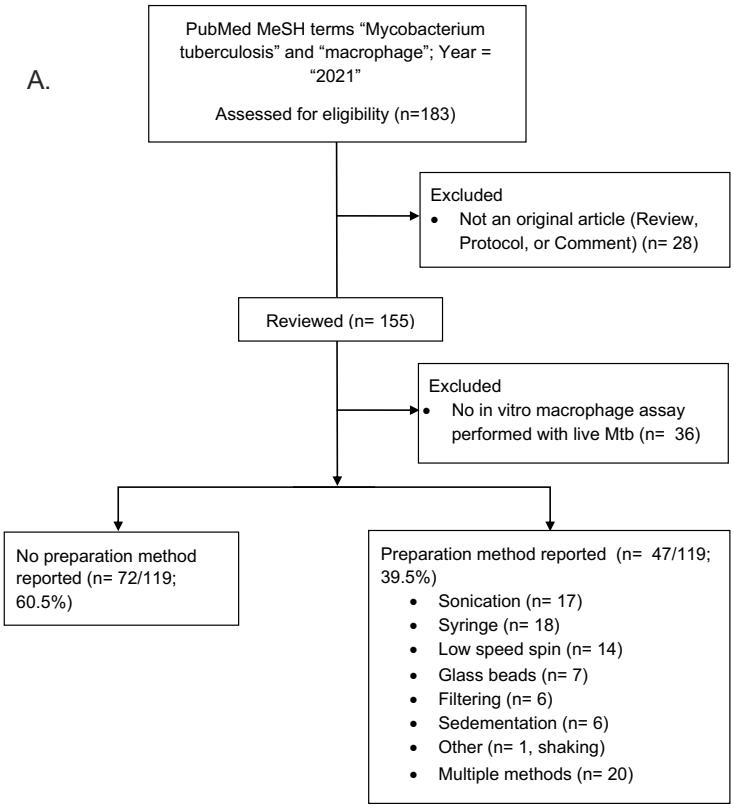

B.

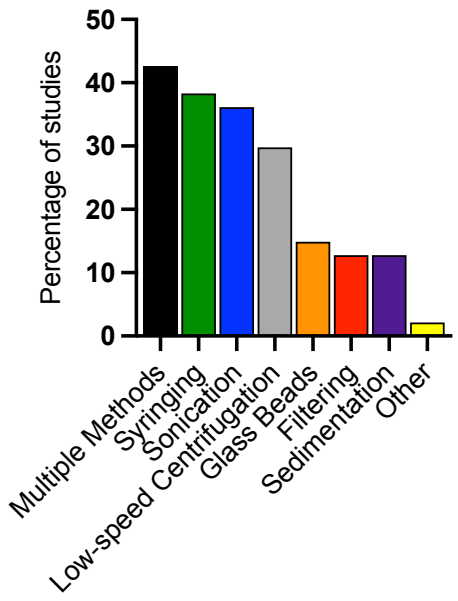

Supplemental Figure 4. Literature review of methods used to generate single cell Mtb suspensions

(**A**) Approach used to analyze the literature to define the frequency with which distinct single cell preparation methods are used and how often they are reported. (**B**) Graph demonstrates the distribution of methods reported. Since some studies used multiple methods, the total does not equal 100.